People's Democratic Republic of Algeria
Ministry of Higher Education and Scientific Research

University M'Hamed BOUGARA – Boumerdes

Institute of Electrical and Electronic Engineering
Department of Power and Control Engineering

Final Year Project Report Presented in Partial Fulfilment of the Requirements for the Degree of

MASTER

In **Power Engineering**

Option: **Power Engineering**

Title:

Vector and Direct Torque Control of Two Induction motors fed by a Single Nine Switch Inverter

Presented by:

- **BOUANZOUL Hamza**
- **GOUBA Omar**

Supervisor:

Pr. KHELDOUN Aissa

Registration Number:………/2020

Abstract

Over the past few years, there has been increasing interest and activity in the field of power electronics and drives, to satisfy the demand of the industrial area where the need for low cost, compact, integrated and reduced component power converters is critical. Nine-switch inverter (NSI) is a compact dual-output inverter developed to control two AC loads with less switches.

Induction motors are very important loads that can be driven independently using nine switch inverters because they are cheap, rugged and require less maintenance, due to these characteristics, they have dominated in the field of electromechanical energy conversion, Nowadays, a large number of induction motors are found in the industry. The nine-switch inverter can serve the role of the dual output inverter that has been used in the past few years for controlling two induction motors, the cost and switching losses can be reduced as the number of switches is reduced from twelve to nine switches only.

In this context, two control techniques; indirect rotor field-oriented control and direct torque control, are investigated in this project to study the independency of control of the nine-switch inverter powered motors. Furthermore, the effectiveness of the developed controllers in separating between the flux and torque control will be checked. Simulations of these techniques are then carried out using MATLAB and the obtained results analyzed and discussed to confirm the validity of the proposed techniques.

Dedication

I would like to dedicate this work:

To my father and my mother for their support

To my brothers and my sister

To all my family and friends

BOUANZOUL Hamza

I would like to dedicate this work:

To my beloved parents, brothers and sisters, may god protect them

To my dear friends whoever helped to achieve this work.

GOUBA Omar

Acknowledgement

First and foremost, praises and thanks to Allah, the Almighty, for his conciliation in the completion of this humble work.

We are sincerely obliged to many worthy persons, without whom we could have never had the opportunity of learning greatly with interest. Special gratitude goes to our enthusiastic and amazing supervisor, **Pr. A. KHELDOUN** whose guidance has been present every step of our final project study.

We also would like to extend our most profound appreciations to the jury members for offering us time in reading our project report.

Last but by no means least, thanks go to our parents for their love, prayers, caring and sacrifices for educating and preparing us for the future. They are the most important people in our world and we dedicate this work to them. Also, we express our thanks to our sisters, brothers, grandparents and all our families for their support and valuable prayers.

Table of Content

List of Tables

List of Figures

General Introduction

Induction motors are critical components in many industrial processes. Due to their simple construction, high reliability and low cost, have dominated in the field of electromechanical energy conversion.

Today, Multi-motor systems gain an important place in industry applications such as electric power train, textile paper industries and electric vehicles. Recently, the three important factors to design a suitable control scheme for these systems are reliability, efficiency and economic factors. Hence, many research works have been undertaken to decrease the number of power electronic devices needed in drive systems, which leads to reducing the complexity of the system, therefore the cost and efficiency of the overall system enhanced.

Our project deals with driving two induction motors power by nine-switch inverter independently. Two control techniques are investigated; indirect field-oriented control technique (IRFOC) with sinusoidal pulse width modulation technique SPWM and Direct torque control DTC with switching table are used.

For this, the report is organised in four chapters, theoretical background and mathematical modeling of induction motor are illustrated in the first chapter. Then the second chapter deals with the nine switch inverter, principle of operation and various techniques of PWM applied to it. Simulation of vector controlled nine switch fed induction motors together with results discussion are presented in the third chapter. The fourth chapter is devoted to Direct torque control (DTC) of two induction motor fed by nine switch inverter. A general conclusion summarizes the outcomes of this project.

Chapter One

Modeling of Induction Motor

Chapter 1: Modeling of Induction Motor

1.1 Introduction

An induction motor also known as an asynchronous motor is a commonly used AC electric motor. In an induction motor, the electric current in the rotor needed to produce torque is obtained via electromagnetic induction from the rotating magnetic field of the stator winding. The rotor of an induction motor can be a squirrel cage rotor or wound type rotor.

Three-phase squirrel-cage induction motors are widely used as industrial drives due to many advantages such as low cost, self-starting and more reliable compared to other types of motors. Single-phase induction motors are used widely for in household applications due to its robustness and simple construction and their capability for being attached to grid without using converters.

Induction motors are increasingly being used with variable-frequency drives (VFD) in variable-speed service. VFDs offer especially important energy savings opportunities for existing and prospective induction motors in variable-torque centrifugal fan, pump and compressor load applications. Squirrel cage induction motors are very widely used in both fixed-speed and variable-frequency drive applications.

1.2 Basic construction

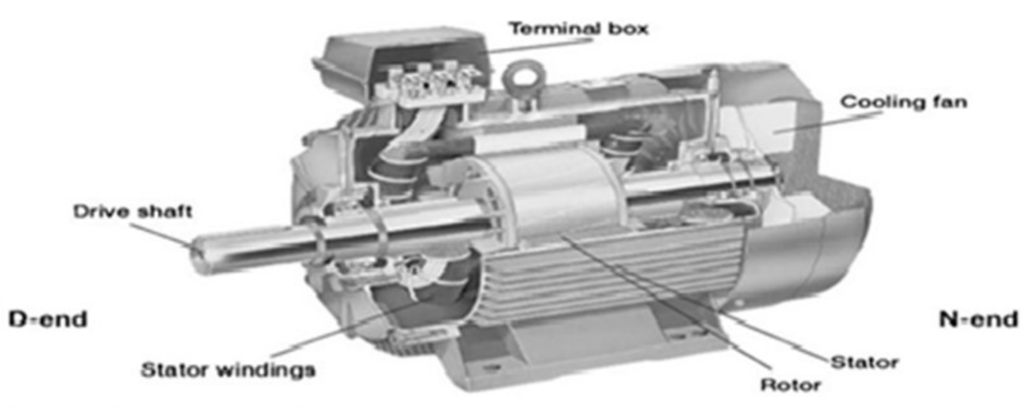

Figure 0.1:An induction motor.

1.2.1 Stator

The stator is the outer stationary part of the motor. It consists of the outer cylindrical frame, the magnetic path, and a set of insulated electrical windings.

- **The outer cylindrical frame**: It is made either of cast iron or cast aluminum alloy or welded fabricated sheet steel. This includes normally feet for foot mounting of the motor or a flange for any other types of mounting of the motor;
- **The magnetic path**: It comprises a set of slotted high-grade alloy steel laminations supported into the outer cylindrical stator frame. The magnetic path is laminated to reduce eddy current losses and heating;
- **A set of insulated electrical windings**: For a 3-phase motor, the stator circuit has three sets of coils, one for each phase, which is separated by 120° and is excited by a three-phase supply. These coils are placed inside the slots of the laminated magnetic path.

1.2.2 Rotor

It is the rotating part of the motor. It is placed inside the stator bore and rotates coaxially with the stator. Like the stator, rotor is also made of a set of slotted thin sheets, called laminations, of electromagnetic substance (special core steel) pressed together in the form of a cylinder. Thin sheets are insulated from each other by means of paper, varnish. Slots consist of the electrical circuit and the cylindrical electromagnetic substance acts as magnetic path. Rotor winding of an induction motor may be of two types:

Squirrel-cage type induction motor: Here rotor comprises a set of bars made of either copper or aluminum or alloy as rotor conductors which are embedded in rotor slots. This gives a very rugged construction of the rotor. Rotor bars are connected on both ends to an end ring to make a close path;

Wound-rotor type induction motor: In this case rotor conductors are insulated windings which are not shorted by end rings but the terminals of windings are brought out to connect them to three numbers of insulated slip rings which are mounted on the shaft. External electrical connections to the rotor are made through brushes placed on the slip rings. For the presence of these slip rings this type of motor is also called slip ring induction motor [1] [2].

Besides the above two main parts, an induction motor consists some other parts which are named as follows

1.2.3 End flanges

There are two end flanges which are used to support the two bearings on both the ends of the motor.

1.2.4 Bearings

There are two set of bearings which are placed at both the ends of the rotor and are used to support the rotating shaft.

1.2.5 Shaft

It is made of steel and is used to transmit generated torque to the load.

1.2.6 Cooling fan

It is normally located at the opposite end of the load side, called non-driving end of the motor, for forced cooling of the both stator and rotor.

1.2.7 Terminal box

It is on top or either side of the outer cylindrical frame of stator to receive the external electrical connections.

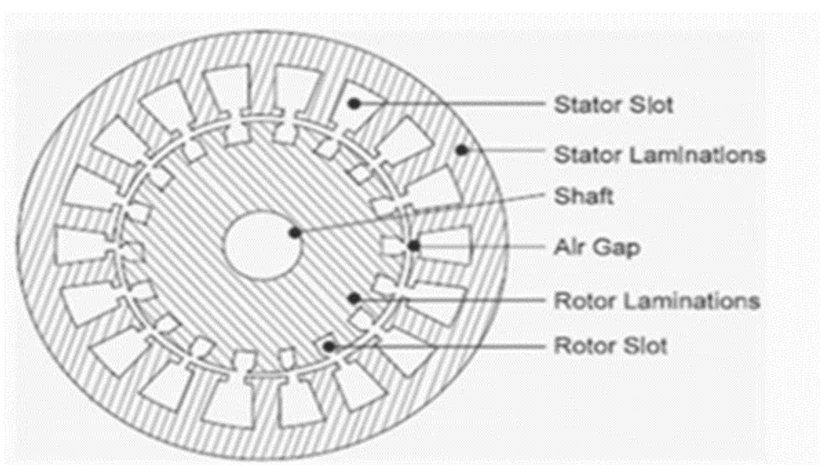

Figure 0.2:Magnetic circuit of stator and rotor of an induction motor.

1.3 Principle of operation

An induction motor consists of two main parts stator and rotor. The stationary or outer part is called stator while rotating part from which we get the mechanical output is called rotor. Like any other machine, induction motor is also an electromechanical device.

As we call it an 'induction' motor, the working principle is simply based on electromagnetic induction. The stator of the machine houses coils on it while rotor is cylindrical and carries conductor bars. When AC supply is given, it excites the stator coils. Now, AC supply is time varying and we know a time varying current through a coil produces time varying magnetic flux which can induce emf in a nearby conductor. Between stator and rotor remains a very small air gap. Thus, stator produces a time varying magnetic field in this air gap. For a 3-phase stator coil it can be shown that the generated magnetic field is a rotating one.

This rotating magnetic field flux is cut by the rotor conductor bar which induces emf through them. As we know from Lenz's law, the induced emf is so as to oppose the very cause of its own creation. Thus, the rotor induced emf tries to reduce the effect of stator air gap rotating magnetic field flux by trying to rotate at the same speed as that of the magnetic field. In other way, the rotor tries to achieve a speed where relative velocity between rotor and the rotating air gap flux becomes zero (although never happens) [3].

1.4 Motor equivalent circuit

One way to analyze and understand the operation of an induction motor is by the use of an equivalent circuit, an induction motor is similar in action to transformer with rotating secondary windings.

From the preceding we can utilize the equivalent circuit of transformer to model an induction motor.

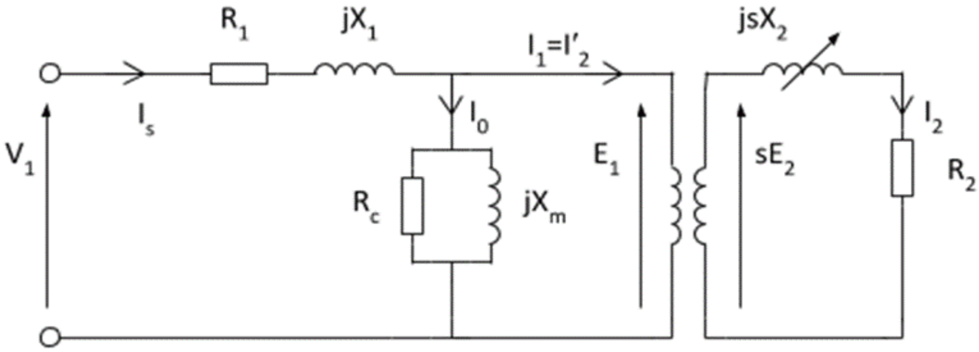

Figure 0.3:An induction motor equivalent circuit

In the equivalent circuit R_1 represents, the resistance of the stator winding and X_1 the stator leakage reactance (flux that does not link with the air gap and rotor). Magnetizing reactance required to cross the air gap is represented by X_m and core losses (hysteresis and eddy current) by R_c.

An ideal transformer of N_1 and N_2 turns respectively represents the air gap. For the rotor side, the induced emf is affected by the slip (as the rotor gains speed, slip reduces and less emf is induced).

The rotor resistance and reactance are represented by R_2 and X_2 ;with X_2 being dependent on the frequency of the inductor rotor emfs.

The rotor circuit, the current $I_2$is given by:

$$I_2 = \frac{sE_2}{\sqrt{(R_2)^2 + (sX_2)^2}} \tag{1.1}$$

which can be rewritten as:

$$I_2 = \frac{E_2}{\sqrt{\left(\frac{R_2}{s}\right)^2 + (X_2)^2}} \tag{1.2}$$

The above equality allows the equivalent circuit to be drawn as:

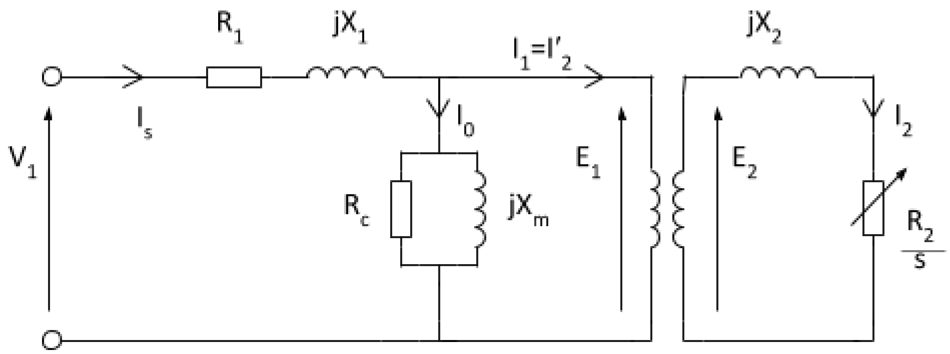

Figure 0.4:A simplified induction motor equivalent circuit.

1.5 Torque speed curve

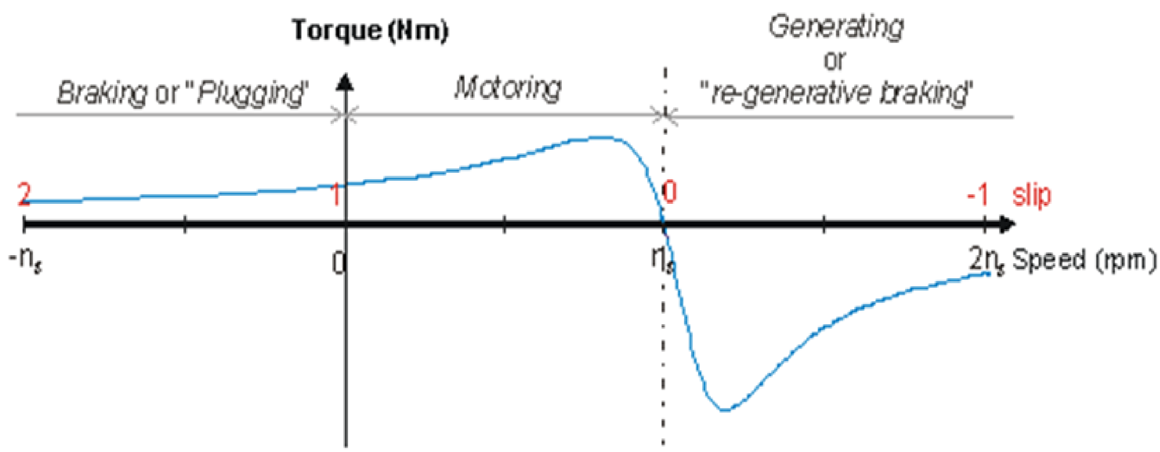

Figure 0.5:Torque-speed curve of induction motor.

The torque-speed curve brakes down into three operating regions:

1. **Braking**, $nm < 0, s > 1$

   Torque is positive whilst speed is negative. Considering the power conversion equation

$$P_{conv} = (1 - s)P_{gap} \tag{1.3}$$

It can be seen that if the power converted is negative (from P=τω) then the airgap power is positive. i.e. the power is flowing from the stator to the rotor and also into the rotor from the mechanical system. This operation is also called plugging.

This mode of operation can be used to quickly stop a machine. If a motor is travelling forwards it can be stopped by interchanging the connections to two of the three phases. Switching two phases has the result of changing the direction of motion of the stator magnetic field, effectively putting the machine into braking mode in the opposite direction.

2. **Motoring,** $0 < nm < ns, 0 < s < 1$

Torque and motion are in the same direction. This is the most common mode of operation.

3. **Generating**, $nm > ns, s < 0$

In this mode, again torque is positive whilst speed is negative. However, unlike plugging,

$$P_{conv} = (1 - s)P_{gap} \tag{1.4}$$

Indicates that if the power converted is negative, so is the air gap power. In this case, power flows from the mechanical system, to the rotor circuit, then across the air gap to the stator circuit and external electrical system.

1.6 Mathematical modeling of induction motor

The dynamic model of induction motor is based on three phases-two phases Park's transformation which is used to determine the model of the motor d-q reference frame. The state equations of induction motor with four electrical variables (currents and fluxes), a mechanical variable (rotor speed).

In this work, state space equations of the machine in rotating frame are considered with flux linkages as the main variables.

Three phase voltages supplied to the motor are as follows

$$V_{as} = V_m sin(\omega_e t) \tag{1.5}$$

$$V_{bs} = V_m sin(\omega_e t - \frac{2\pi}{3}) \tag{1.6}$$

$$V_{cs} = V_m sin(\omega_e t + \frac{2\pi}{3}) \tag{1.7}$$

V_m is the amplitude of terminal voltage and we is the supply frequency.

To develop dynamic model of induction motor, the three phases to two axis transformation is needed

$d - q$ Transformation :

$$V_{qss} = \frac{\sqrt{2}}{3}\left(-sin(\theta) * V_a - sin\left(\theta - \frac{2\pi}{3}\right) * V_b - sin\left(\theta + \frac{2\pi}{3}\right) * V_c\right) \quad (1.8)$$

$$V_{dss} = \frac{\sqrt{2}}{3}\left(cos(\theta) * V_a + cos\left(\theta - \frac{2\pi}{3}\right) * V_b + cos\left(\theta + \frac{2\pi}{3}\right) * V_c\right) \quad (1.9)$$

Then the two-phase stationary reference frame variables are transformed into two phase synchronously rotating frame variables this is achieved by following equations

$$V_{qs} = V_{qss}\cos(\theta) - V_{dss}\sin(\theta) \quad (1.10)$$

$$V_{ds} = Vqss * sin(\theta) + Vdss * cos(\theta) \quad (1.11)$$

θ is the angle of rotating frame with respect to stationary frame

$$V_{qss} = R_s\, i_{qs} + \frac{d\Psi qs}{dt} \quad (1.12)$$

$$V_{dss} = R_s\, i_{ds} + \frac{d\Psi ds}{dt} \quad (1.13)$$

Where Ψ_{qs} and Ψ_{ds} are stator flux linkages of q-axis and d-axis respectively. After converting above equations to synchronously rotating de-qe frame, we get following equations.

$$V_{qs} = R_s\, i_{qs} + \frac{d\Psi qs}{dt} + \omega\Psi_{\mathrm{ds}} \quad (1.14)$$

$$V_{ds} = R_s\, i_{ds} + \frac{d\Psi ds}{dt} - \omega\Psi_{\mathrm{qs}} \quad (1.15)$$

The rotor circuit equations are given by

$$V_{qr} = R_r\, i_{qr} + \frac{d\Psi qr}{dt} + \omega\Psi_{\mathrm{dr}} \quad (1.16)$$

$$V_{dr} = R_s\, i_{dr} + \frac{d\Psi dr}{dt} - \omega\Psi_{\mathrm{qr}} \quad (1.17)$$

The rotor actually moves at speed ω_r. Therefore, the d-q axes fixed on the rotor move at speed relative to $(\omega_e - \omega_r)$ synchronously rotating frame. Therefore, in de-qe frame, the actual rotor equations are written as follows

$$V_{qr} = R_r\, i_{qr} + \frac{d\Psi qr}{dt} + (\omega_e - \omega_r)\,\Psi_{\mathrm{dr}} \tag{1.18}$$

$$V_{dr} = R_r\, i_{dr} + \frac{d\Psi dr}{dt} - (\omega_e - \omega_r)\,\Psi_{\mathrm{qr}} \tag{1.19}$$

As earlier said, in this work dynamic model of induction motor in state space form is going is developed. Therefore, it is necessary to define flux linkage variables and is given as follows

$$F_{qs} = \omega_b\, \Psi_{qs} \tag{1.20}$$

$$F_{qr} = \omega_b\, \Psi_{qr} \tag{1.21}$$

$$F_{ds} = \omega_b\, \Psi_{ds} \tag{1.22}$$

$$F_{dr} = \omega_b\, \Psi_{dr} \tag{1.23}$$

Where:

ω_b is base frequency of the machine. Substituting the relations in stator and rotor equations, we get the following equations assuming $V_{qr} = V_{dr} = 0$.

$$V_{qs} = R_s\, i_{qs} + \frac{1}{\omega_b}\left(\frac{dF_{qs}}{dt}\right) + \left(\frac{\omega_e}{\omega_b}\right) F_{ds} \tag{1.24}$$

$$V_{ds} = R_s\, i_{qds} + \frac{1}{\omega_b}\left(\frac{dF_{ds}}{dt}\right) - \left(\frac{\omega_e}{\omega_b}\right) F_{qs} \tag{1.25}$$

$$R_{\mathrm{r}}\, i_{\mathrm{qr}} + \frac{1}{\omega_b}\left(\frac{dF_{\mathrm{qr}}}{dt}\right) + \frac{(\omega_e - \omega_r)}{\omega_b}\, F_{\mathrm{dr}} = 0 \tag{1.26}$$

$$R_r\, i_{dr} + \frac{1}{\omega_b}\left(\frac{dF_{dr}}{dt}\right) - \frac{(\omega_e - \omega_r)}{\omega_b}\, F_{qr} = 0 \tag{1.27}$$

Multiplying equations by ωb on both sides, the flux linkage expressions can be written as

$$F_{qs} = \omega b\, \Psi_{qs} = \mathrm{Xls}\, i_{qs} + \mathrm{Xm}(i_{qs} + i_{qr}) \tag{1.28}$$

$$F_{qr} = \omega b\, \Psi_{qr} = \mathrm{Xlr}\, i_{qr} + \mathrm{Xm}(i_{qs} + i_{qr}) \tag{1.29}$$

$$F_{qm} = \omega b\, \Psi_{qm} = \mathrm{Xm}(i_{qs} + i_{qr}) \tag{1.30}$$

$$F_{ds} = \omega b\, \Psi_{ds} = \mathrm{Xls}\, i_{ds} + \mathrm{Xm}(i_{ds} + i_{dr}) \tag{1.31}$$

$$F_{dr} = \omega b\, \Psi_{dr} = \mathrm{Xlr}\, i_{qr} + \mathrm{Xm}(i_{qs} + i_{qr}) \tag{1.32}$$

$$F_{dm} = \omega b\, \Psi_{dm} = \mathrm{Xm}(i_{qr} + i_{qr}) \tag{1.33}$$

Where: $Xls = \omega b * Lls$: Stator leakage reactance

$Xlr = \omega b * Llr$: Rotor leakage reactance

$Xm = \omega b * Lm$: Magnetizing Reactance

But,

$$F_{qs} = \mathrm{Xls}\, i_{qs} F_{qm}) \tag{1.34}$$

$$F_{qr} = \mathrm{Xlr}\, i_{qr} + F_{qm} \tag{1.35}$$

$$F_{ds} = \mathrm{Xls}\, i_{ds} + F_{dm} \tag{1.36}$$

$$F_{dr} = \mathrm{Xlr}\, i_{ds} + F_{dm} \tag{1.37}$$

Now, currents can be expressed in terms of flux linkages as follows

$$i_{qs} = \frac{F_{qs} - F_{qm}}{Xls} \tag{1.38}$$

$$i_{qr} = \frac{F_{qr} - F_{qm}}{Xlr} \tag{1.39}$$

$$i_{ds} = \frac{F_{ds} - F_{dm}}{Xls} \tag{1.40}$$

$$i_{dr} = \frac{F_{dr} - F_{dm}}{Xlr} \tag{1.41}$$

F_{qm} and F_{dm} are written as

$$F_{qm} = Xm\left(\frac{F_{qs} - F_{qm}}{Xls} + \frac{F_{qr} - F_{qm}}{Xlr}\right) \tag{1.42}$$

$$F_{dm} = Xm\left(\frac{F_{ds} - F_{dm}}{Xls} + \frac{F_{dr} - F_{dm}}{Xlr}\right) \tag{1.43}$$

The stator and rotor voltage equations can be written after substituting equations (1.44) to (1.47) in equations (1.24) to (1.27) as follows

$$V_{qs} = \frac{R_S}{Xls}\left(F_{qs} - F_{qm}\right) + \frac{1}{\omega b} * \frac{dF_{qs}}{dt} + \frac{\omega e}{\omega b}F_{ds} \tag{1.44}$$

$$V_{ds} = \frac{R_S}{Xls}(F_{ds} - F_{dm}) + \frac{1}{\omega b} * \frac{dF_{ds}}{dt} - \frac{\omega e}{\omega b}F_{qs} \tag{1.45}$$

$$0 = \frac{R_r}{Xlr}\left(F_{qr} - F_{qm}\right) + \frac{1}{\omega b} * \frac{dF_{qr}}{dt} + \frac{\omega e - \omega r}{\omega b}F_{dr}) \tag{1.46}$$

$$0 = \frac{R_r}{Xlr}(F_{dr} - F_{dm}) + \frac{1}{\omega b} * \frac{dF_{dr}}{dt} - \frac{\omega e - \omega r}{\omega b}F_{qr} \tag{1.47}$$

Now, the above equations can be modified to express in state space form as follows

$$\frac{dF_{qs}}{dt} = \omega b\ (Vqs - \frac{\omega e}{\omega b}F_{ds} + \frac{R_s}{Xls}(F_{qr}\frac{Xm}{Xlr} + F_{qs}\left(\frac{Xm}{Xls} - 1\right))) \tag{1.48}$$

$$\frac{dF_{ds}}{dt} = \omega b\ (Vds - \frac{\omega e}{\omega b}F_{qs} + \frac{R_s}{Xls}(F_{dr}\frac{Xm}{Xlr} + F_{ds}\left(\frac{Xm}{Xls} - 1\right))) \tag{1.49}$$

$$\frac{dF_{qr}}{dt} = \omega b\ (-\frac{(\omega e - \omega r)}{\omega b}F_{dr} + \frac{R_r}{Xlr}(F_{qs}\frac{Xm}{Xls} + F_{qr}\left(\frac{Xm}{Xls} - 1\right))) \tag{1.50}$$

$$\frac{dF_{dr}}{dt} = \omega b\ (\frac{(\omega e - \omega r)}{\omega b}F_{qr} + \frac{R_r}{Xlr}(F_{ds}\frac{Xm}{Xlr} + F_{dr}\left(\frac{Xm}{Xls} - 1\right))) \tag{1.51}$$

After finding state variables and currents, finally electromagnetic torque produced by the motor is found by following equation

$$Te = \frac{3}{2}\frac{2}{P}\frac{1}{\omega b}\left(F_{ds}i_{qs} - F_{qs}i_{ds}\right) \tag{1.52}$$

Once the torque is found, the speed of the motor can be calculated by the equation

$$Te = Tl + \frac{2}{P}J\frac{d\omega r}{dt} \tag{1.53}$$

Where:

Tl: is load torque which is given by a step signal in this simulation;

P: is the number of poles;

J: is the rotor inertia;

ωr : is the rotor speed in rad/sec.

1.7 Simulation of induction motor using SIMULINK/MATLAB

Based on mathematical modeling of induction motor listed in previous section, we built a global Simulink/MATLAB model listed below

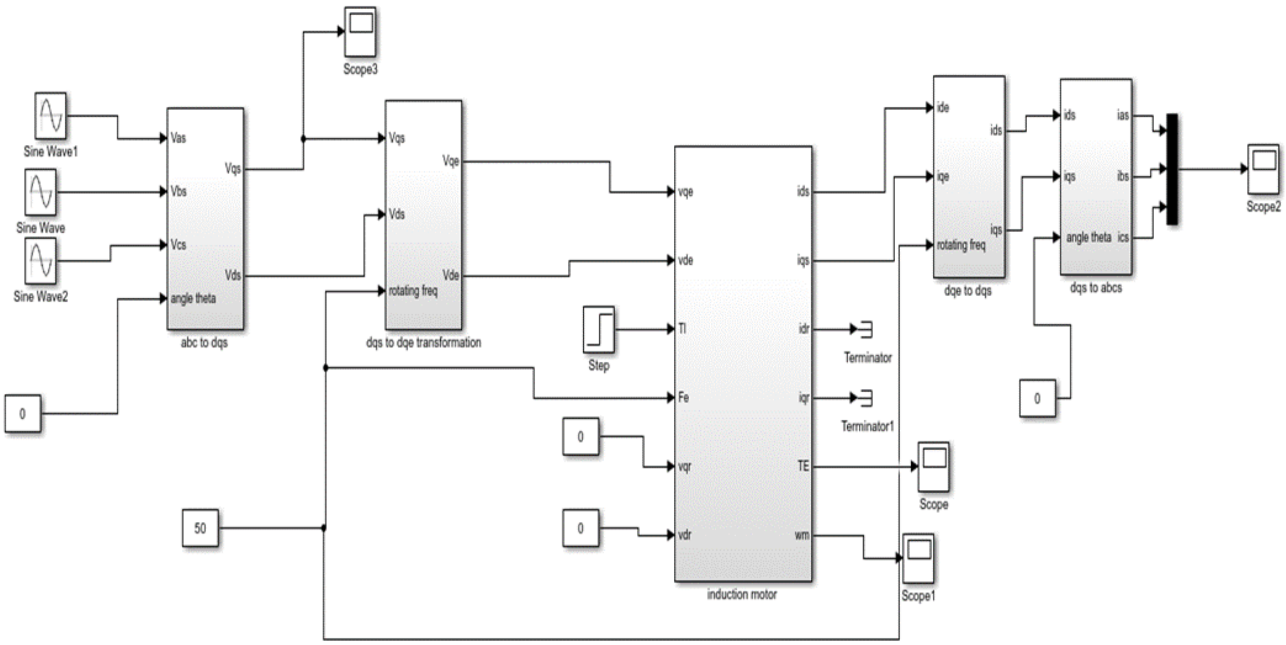

Figure 0.6:Simulink model of induction motor.

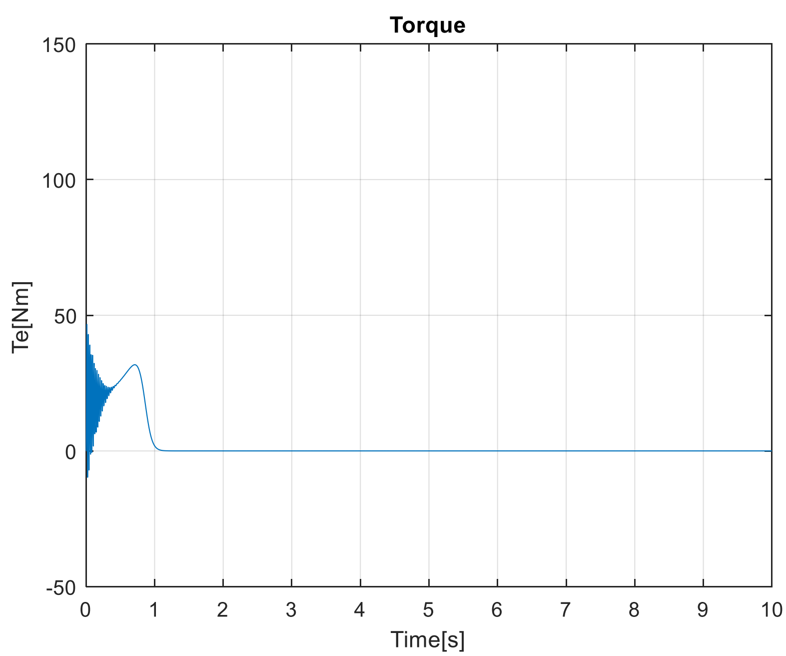

Figure 0.7:Electromagnetic torque of induction motor under no load

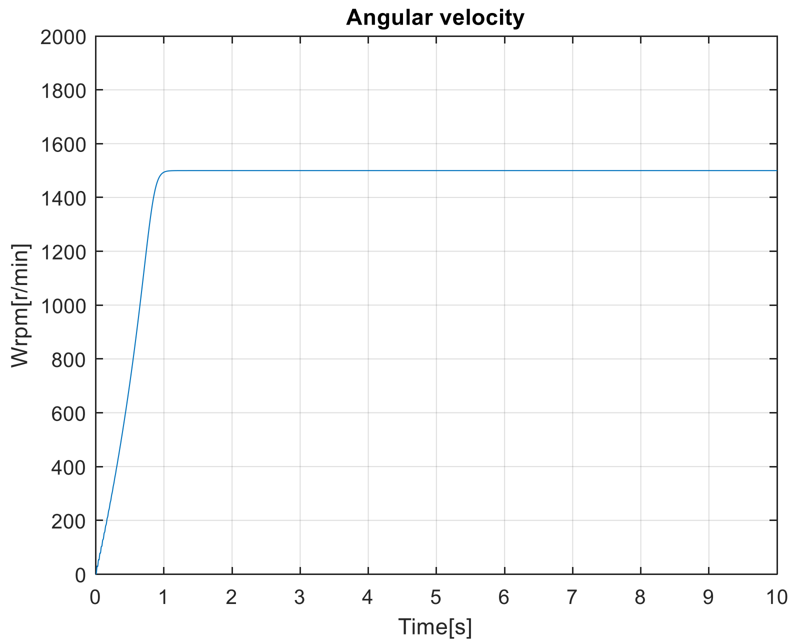

Figure 0.8:Angular speed of induction motor under no load

In this part, we have presented a Simulink model for healthy induction motor. Two phase stationary axis and rotating frame currents are obtained. This induction motor model not only can be used alone but also can be used in high performance motor drive systems such as field-oriented control of induction motor, sensorless speed control of induction motor.

1.8 Conclusion

In this chapter, we dealt with theoretical background on induction motor: construction, principle of operation, torque speed curve and modulization which are necessary background for speed and torque control of induction motor.

Chapter Two

Nine switch inverter (NSI)

Chapter 2: Nine switch inverter (NSI)

2.1 Introduction

Within the last decade, there have been major advancements in power electronics. Power electronics have moved along with these developments with such things as digital signal processors being used to control power systems. An Inverter is basically a converter that converts DC to AC power. A voltage source inverter (VSI) is one that takes in a fixed voltage from a device, such as a dc power supply, and converts it to a variable-frequency AC supply using many techniques such as pulse width modulation (PWM). The inverter's output can be used to drive AC loads such as induction motors.

This chapter presents the theoretical background of the Nine switch inverter, PWM techniques and the MATLAB simulation for the NSI.

2.2 Three phase voltage source full wave inverters:

The topology for the three-phase full wave VSI is shown in figure 2.1

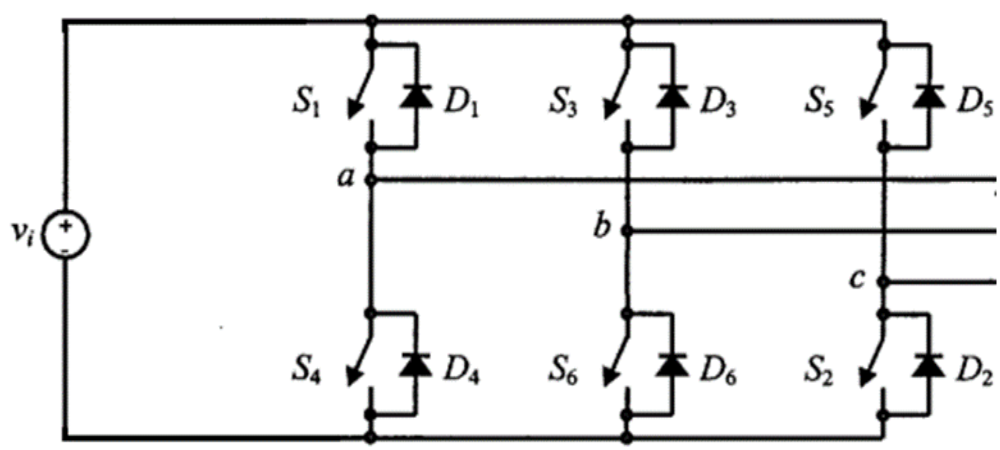

Figure 2.1:Three phase voltage source inverter.

It is composed of six switches (IGBTs or MOSFETs) distributed over three legs with each leg holding two switches, these switches can be controlled using the gate signals to obtain the desired output voltage (line to line or phase voltage).It should be noted that at any time no more than one switch in a leg is turned on to avoid any short circuit across the supply, also the two switches must not be turned off simultaneously as this leads to undefined voltage states.

The relation between the line and phase voltage can be expressed as follows [4]:

$$V_{ab} = \mathrm{V_{an}} - \mathrm{V_{bn}} \tag{2.1}$$

$$V_{bc} = \mathrm{V_{bn}} - \mathrm{V_{cn}} \tag{2.2}$$

$$V_{ca} = \mathrm{V_{cn}} - \mathrm{V_{an}} \tag{2.3}$$

The phase voltages are related to the line voltages by the following equations:

$$V_{an} = \frac{\mathrm{V_{ab}} - \mathrm{V_{ca}}}{3} \tag{2.4}$$

$$V_{bn} = \frac{\mathrm{V_{bc}} - \mathrm{V_{ab}}}{3} \tag{2.5}$$

$$V_{cn} = \frac{\mathrm{V_{ca}} - \mathrm{V_{bc}}}{3} \tag{2.6}$$

The gating signals of the six switches are delayed by 60° from one another and are turned on in the order that is defined by the switch number (from S1 to S6),Figure 2.2 summarizes all the information about the gating signals of the six switches, the line to line voltages and the phase voltages.

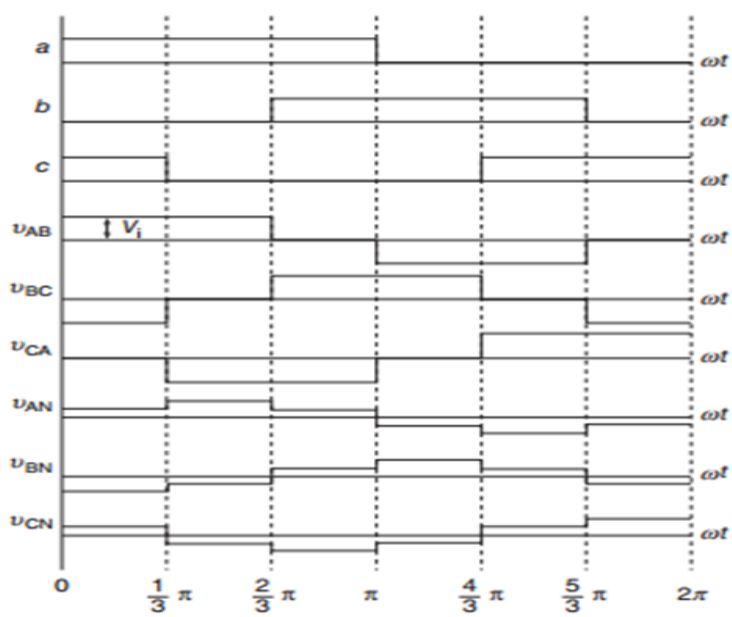

Figure 2.2; The gate pulses of the switches,the line to line voltages and the phase voltages.

The Fourier series representation of line voltages [4] is given by:

$$Vab = \frac{2\sqrt{3}}{\pi}\mathrm{Vdc}\left(\sin\omega t - \frac{1}{5}\sin 5\omega t + \frac{1}{7}\sin 7\omega t\right) + \text{high frequency terms} \qquad (2.7)$$

The remaining line voltages are the same as V_{ab} except for a phase shift of 120°.

The phase voltages are shifted from the line voltage by 30 degree, and their magnitudes are $\frac{2}{\pi}\mathrm{V_{dc}}$ [4].

$$Van = \frac{2}{\pi}\mathrm{Vdc}\left(\sin(\omega t - 30°) - \frac{1}{5}\sin(5\omega t - 30°) + \frac{1}{7}\sin(7\omega t - 30°)\right) + high\ frequency\ terms \qquad (2.8)$$

2.3 Nine switch inverter

The nine-switch inverter is shown in figure 2.3, it has been proposed recently and, since then, a large number of applications have been investigated, especially as a substitute to the dual-bridge (back-to-back) converter. The main advantage of the nine-switch inverter is it has lesser number of switches (nine instead of twelve of the back-to-back converter).

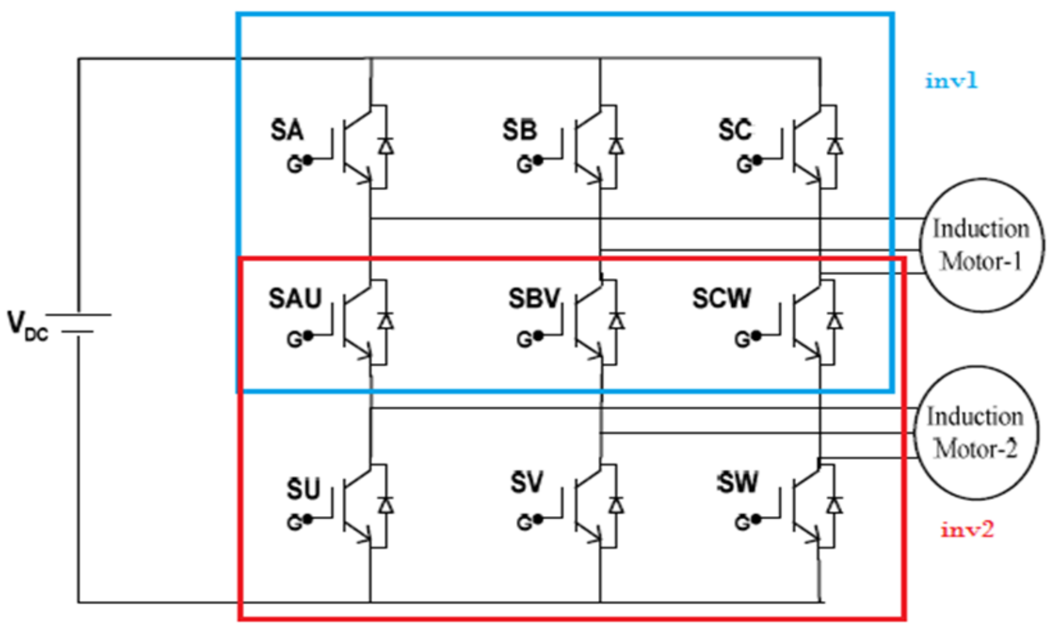

Figure 2.3:The nine-switch inverter topology.

The NSI consists of three arms connected to three switching devices in series. Each phase of motor 1 is connected to the top side of the arm and those of motor 2 are connected to the bottom side. As can be seen from figure 2.3, nine switching devices are employed for the NSI. Therefore, in case of the NSI, three switching devices are reduced as compared to the classical dual output inverter.

The NSI can be viewed as two inverters(inv1,inv2) formed by the upper and lower switches respectively with the middle ones as a common part between the two inverters, the top and bottom switches are called independent switches and their gate signals are generated by comparing two sets of three phase modulating references with either a single carrier or two different carriers, for the case of a single carrier the gating signal for the switch SA is generated by comparing reference signal (VA ref) with the upper half of the triangular waveform. Similarly, by comparing lower reference signal (VU ref) with lower half of the triangular waveform to get the pulse for switch SU. The modulation for upper inverter is in the range 0 to 1 while for lower inverter it is from 0 to -1.

Defining the switching function of a switch as: and

$$S_{ij} = \begin{cases} 1, & \text{switch } S_{ij} \text{ closed} \\ 0, & \text{switch } S_{ij} \text{ open} \\ & (i = A, B, C \text{ and } j = U, V, W) \end{cases}$$

and considering prevention of short circuit and current continuity, the following constraint must be satisfied: Siu + Siv + Siw = 2 From this restriction, we can understand that the NSI has three possible switching states: {1,1,0}, {0,1,1}, {1,0,1} [5].

The switching function describing the nine switch inverter shows that two switches have to be on at a time, and to avoid short circuiting the supply the third switch has to be off, this means that the switching state of the middle switches depend on the top and bottom ones , thus, the gating signals for these switches are generated depending on the states of the two remaining switches for each leg , if the two switches are closed , the remaining switch must be opened , but if only one switch is on the middle switch has to be turn on, this logic gives rise to what is called the ‘’inequality gate’’ or exclusive or function, the output of this gate is 1 if the two inputs are’’ unequal or different “, and 0 if the two inputs are ‘’equal or similar” consequently, The gating signal for the middle switches is obtained by XORing the signal obtained for upper and lower switch. For e.g. Gating pulse for switch SAU is the XOR for the gating use for SA & SU [5]

2.4 PWM techniques for NSI:

2.4.1 SPWM

This control technique for nine- switch inverter employs two sinusoidal reference signals (upper and lower) for each phase. One reference signal (V_U^{ref}) is compared with the upper positive part of the triangular carrier signal to generate the gating signals for the upper switches, similarly, the lower part of the carrier signal is compared with the other reference signal(V_L^{ref}) to obtain the gating pulses for the bottom switches, The gate pulses for the middle switches are generated by the logical XOR of the gate pulses for upper and lower switches. With this method, always two switches are ON in each leg [6]

The two reference signals are given by equations (2.9) and (2.10):

$$V_U{}^{ref} = A.\sin(2.\pi.f_1 t + \alpha_1) \tag{2.9}$$

$$V_L{}^{ref} = B.\sin(2.\pi.f_2 t + \alpha_2) \tag{2.10}$$

A and B represent the amplitudes of the reference signals, f_1 and f_2 are their corresponding frequencies and α_1 and α_2 are their phase angles.

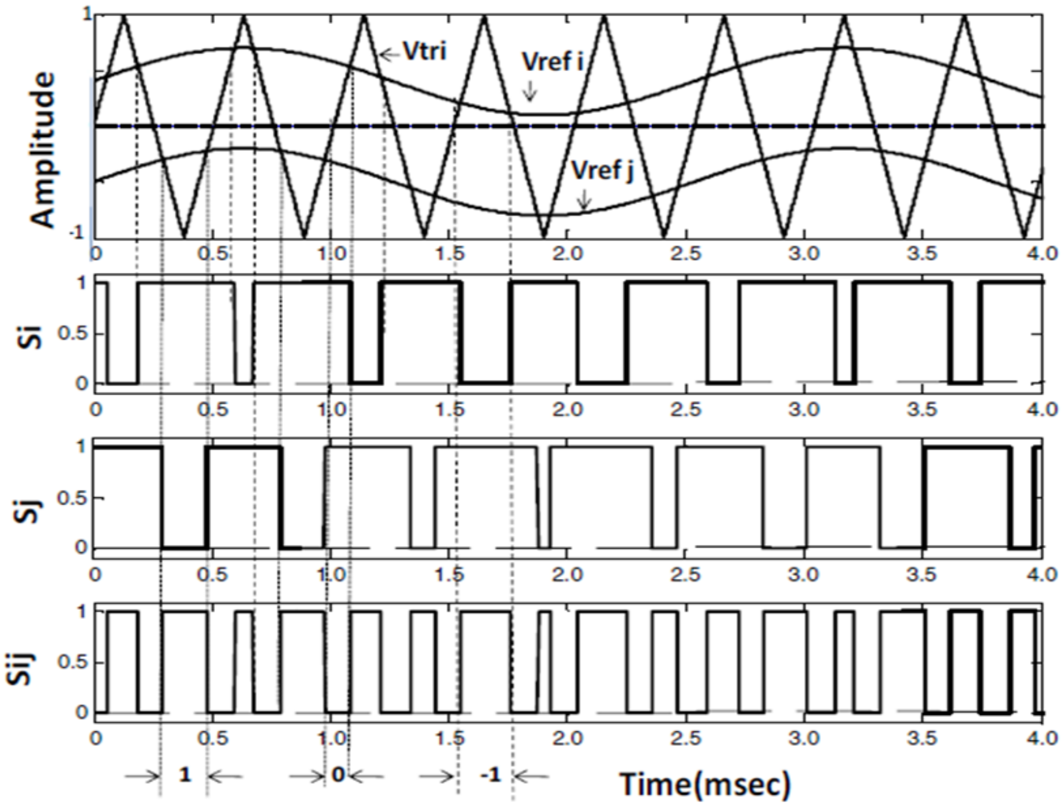

Figure 2.4:The upper reference signal for inv1,the lower reference signal for inv2,triangular carrier and the generated gate signals for switches SA, SU and SAU.

It can be noticed that the pulses for switch Sij is the XOR logic combination of the gating signals for switches Si and Sj.

2.4.2 Space Vector Pulse Width Modulation (SVPWM)

SVPWM is a direct digital technique based on the space vector representation of the reference signal, it uses specific space vectors to find the conduction times of the switching devices required to synthesize the reference variable(voltage, current, flux...) [7].

2.4.2.1 Space vector representation

Any variable in three phase system can be represented in a two-phase stationary frame using Clark Transformation. The resulting space vector rotate at arbitrary speed w. [8]

For

$$\vec{x} = \begin{cases} x_a(t) \\ x_b(t) \\ x_c(t) \end{cases} \quad \text{written as space vector} \quad \vec{x} = \frac{2}{3}\left(x_a(t) + a x_b(t) + a^2 x_c(t)\right)$$

where $a = 1e^{j\frac{2*\pi}{3}}$ and a^2 is its conjugate.

For a balanced three phase stator voltages, the space vector rotates inside a circle of radius equal to the peak of the voltage and speed equal to the angular speed of the sinusoidal voltages.

Before going directly to NSI, the SVPWM is first studied for the three-phase full wave inverter. As discussed earlier, in each leg only one switch is on at a time, so each leg can be in two states, with a total of three legs eight states are possible for the output voltage. Assigning a (1) to a top ON switch and (0) to a top OFF switch. These states are V_0(000), V_1(100), V_2(110), V_3(010), V_4(011), V_5(001), V_6(101), V_7(111).

The state V_1(100) for example is shown in figure 2.5, it is achieved by closing S1, S2, S6 with the remaining switches being opened, this brings point a to V_{dc}, b and c to 0.

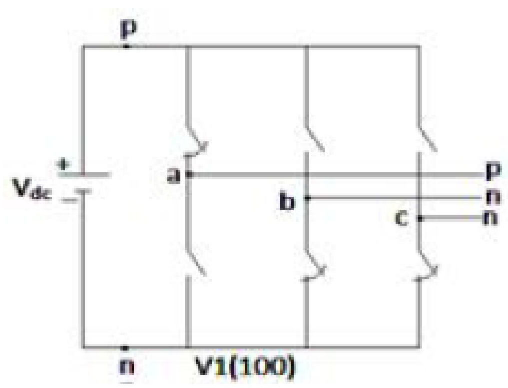

Figure 2.5:The three-phase inverter at state (100).

The resulting space vector is shown in figure 2.5 with $V_g = V_{dc}$

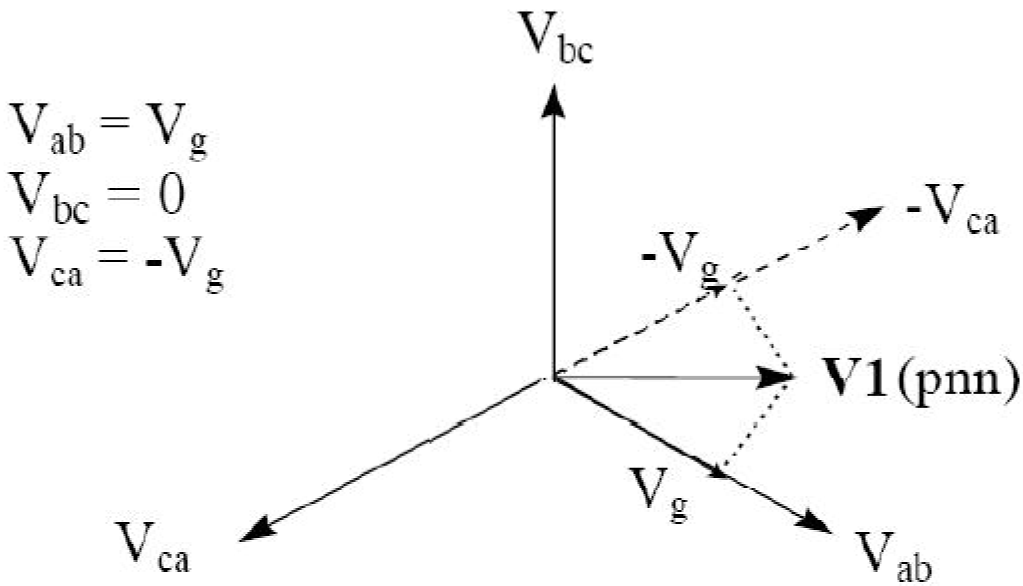

Figure 2.6:Space vector resulting from state (100).

There are two vectors which are called zero vectors, these are V0(000), V7(111) which bring the line to line voltages to zero. The remaining state vectors are called active vectors and they form a hexagon, which is divided in 6 identical sectors with angle of 60° each.

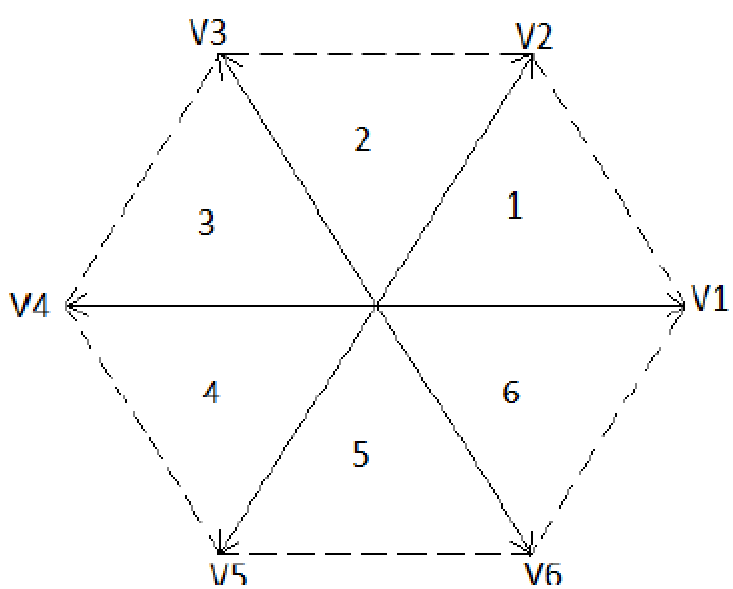

Figure 2.7:The hexagon formed by the active vectors.

Consider a reference vector $\vec{v}$, it can be synthesized using two adjacent active vectors applied for time periods Tx and Ty respectively and one zero vector applied for a time period of Tz during a sampling period of T, in figure 2.8 the vector V lies in the first sector and it is bordered by the vectors V1 and V2.

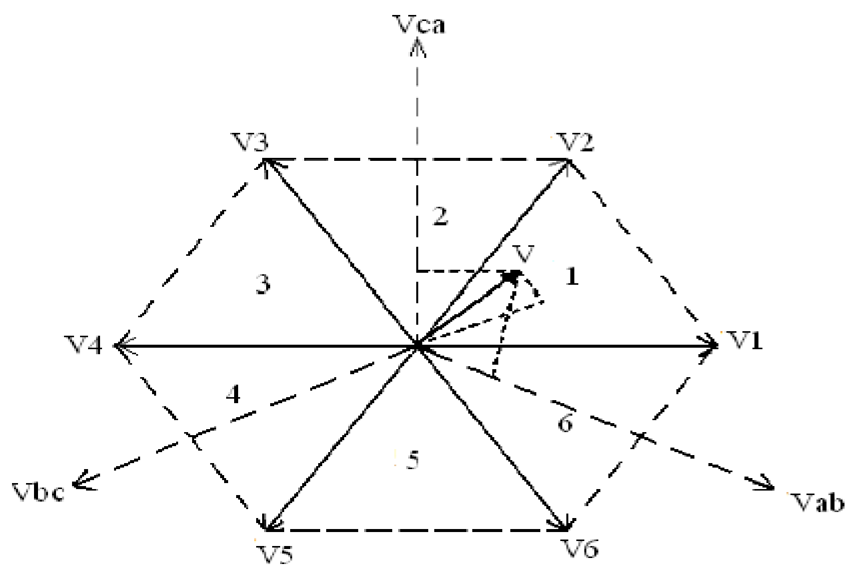

Figure 2.8:The reference vector V space vector representation.

Syntheses of vector V is achieved via sampling V at a sampling period of T, applying the active vectors V_1 and V_2 for time T_1 and T_2 respectively and the zero vectors for the remaining of the sampling time (T_z).

Mathematically, the vector V can be related to its adjacent vectors V_x (the one to the right of V) and V_y (the one to the left of V) by equation (2.11).

$$T_x\, V_x + T_y\, V_y = mTe^{j\theta} \tag{2.11}$$

$$T_x + T_y + T_z = T \tag{2.12}$$

Where m is the modulation index, ɵ is the angle formed by the vector V_x and the vector V being synthesized, the time T_x and T_y are found using equations (2.13)and(2.14)

$$T_x = mT\sin(60 - \theta) \tag{2.13}$$

$$T_y = mT\sin(\theta) \tag{2.14}$$

$$T_z = T - T_x - T_y \tag{2.15}$$

To construct the sampled version of V described in figure 2.9, V_0 is being applied for $\frac{T_z}{2}$ then, V_1 is being applied for time T_x and V_2 for time T_y followed by V_7 for a time of $\frac{T_z}{2}$

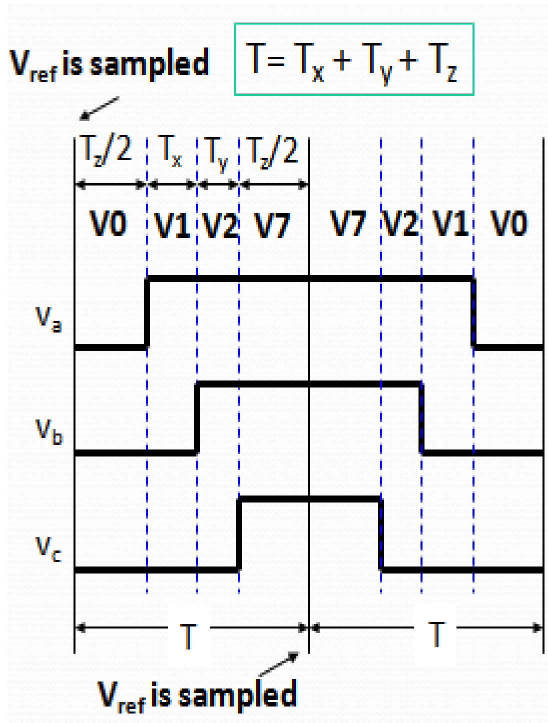

Figure 2.9:Sampled version of the reference signal.

2.5 Simulation results and analysis

This part presents the MATLAB/SIMULINK simulation and results of the SPWM technique for NSI driving two sets of three phase Y connected RL loads.

2.5.1 SPWM technique for NSI using MATLAB/SIMULINK

Figure 2.10 shows the SIMULINK block diagram of the SPWM strategy applied to a NSI connected to two sets of 3 phase Y connected RL loads.

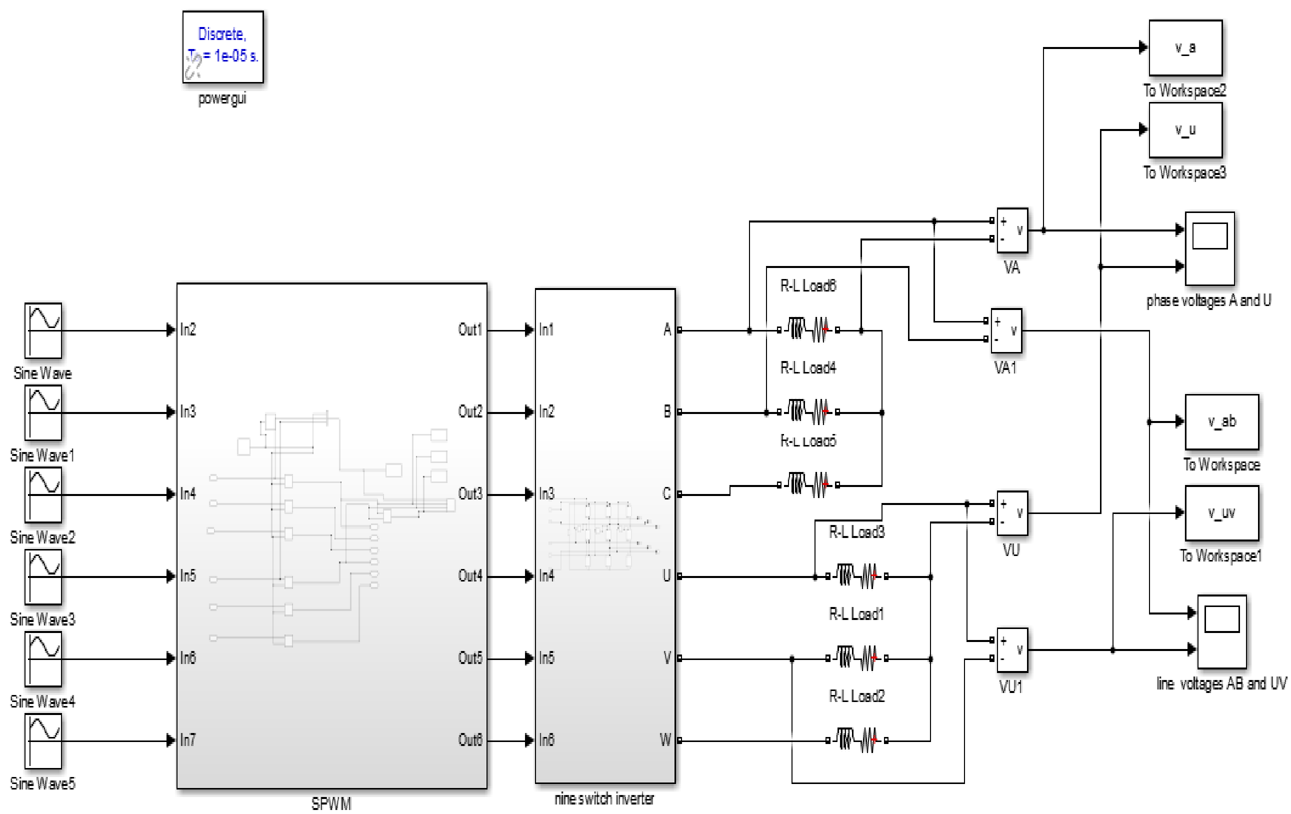

Figure 2.10:General SIMULINK block for SPWM NSI feeding two Y connected three phase RL loads.

The SPWM block content is illustrated in figure 2.12 the carrier frequency is set at 5KHz, the upper reference signals frequency is 25 Hz and the lower reference signals frequency is set at 50 Hz.

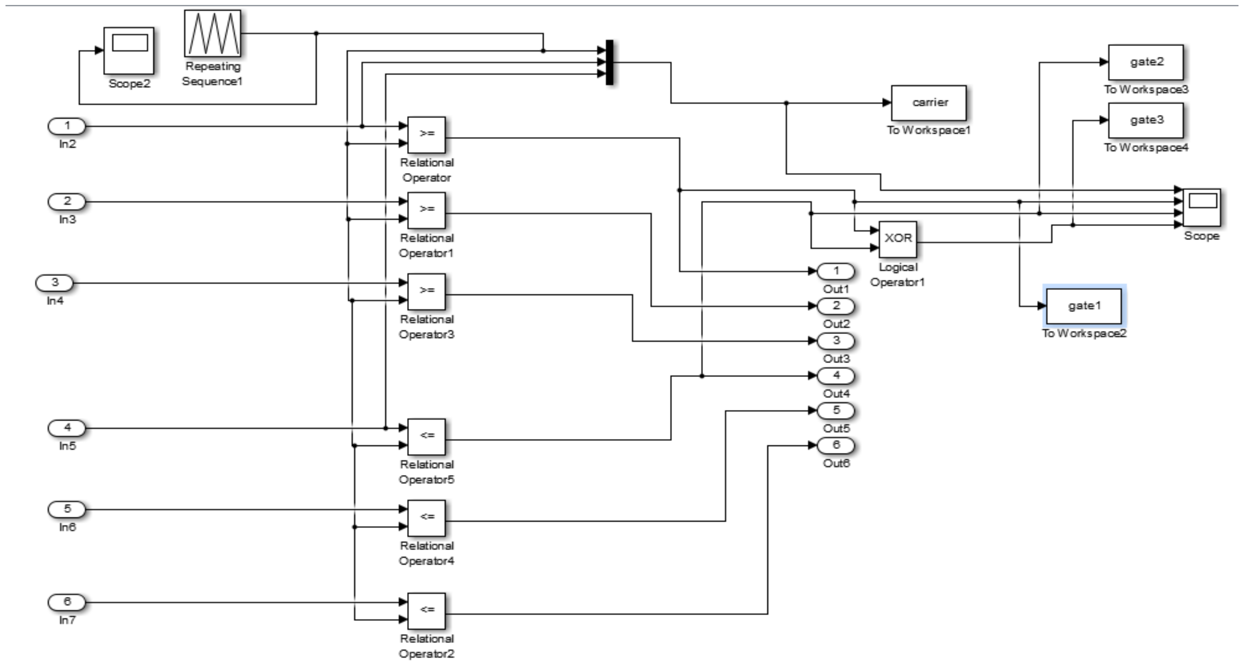

Figure 2.11: SIMULINK block diagram of SPWM technique for NSI.

The building blocks of the nine-switch inverter are illustrated in figure 2.11, the dc link voltage is set at 400V, and the logical XOR operator is used for gating the middle switches.

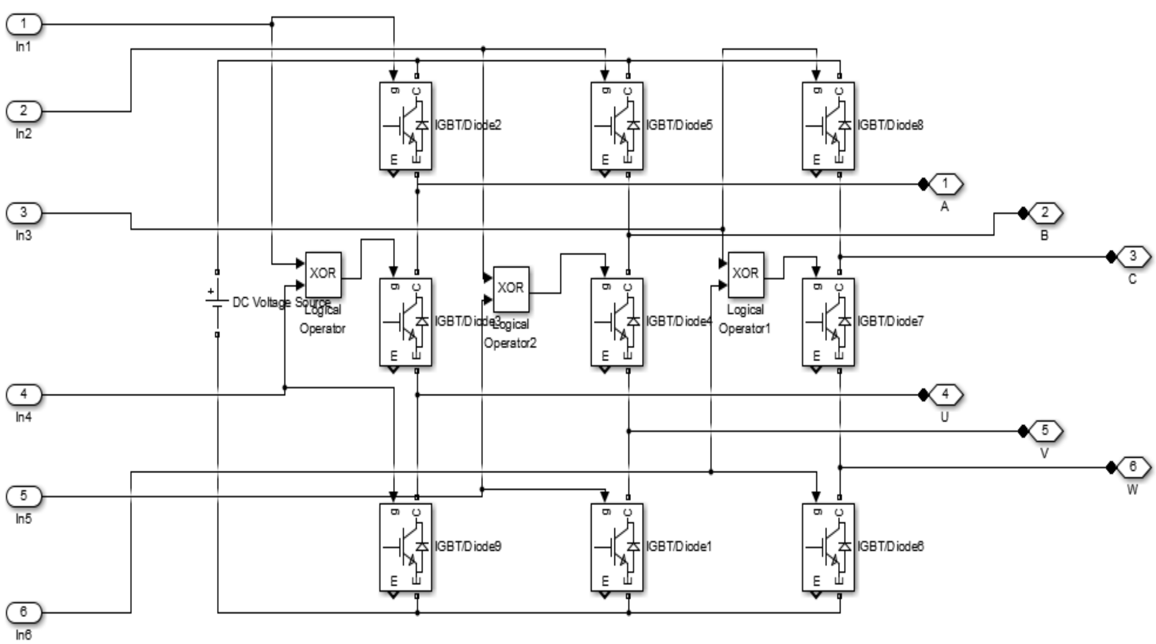

Figure 2.12: SIMULINK block diagram for NSI.

2.5.2 Simulation Results

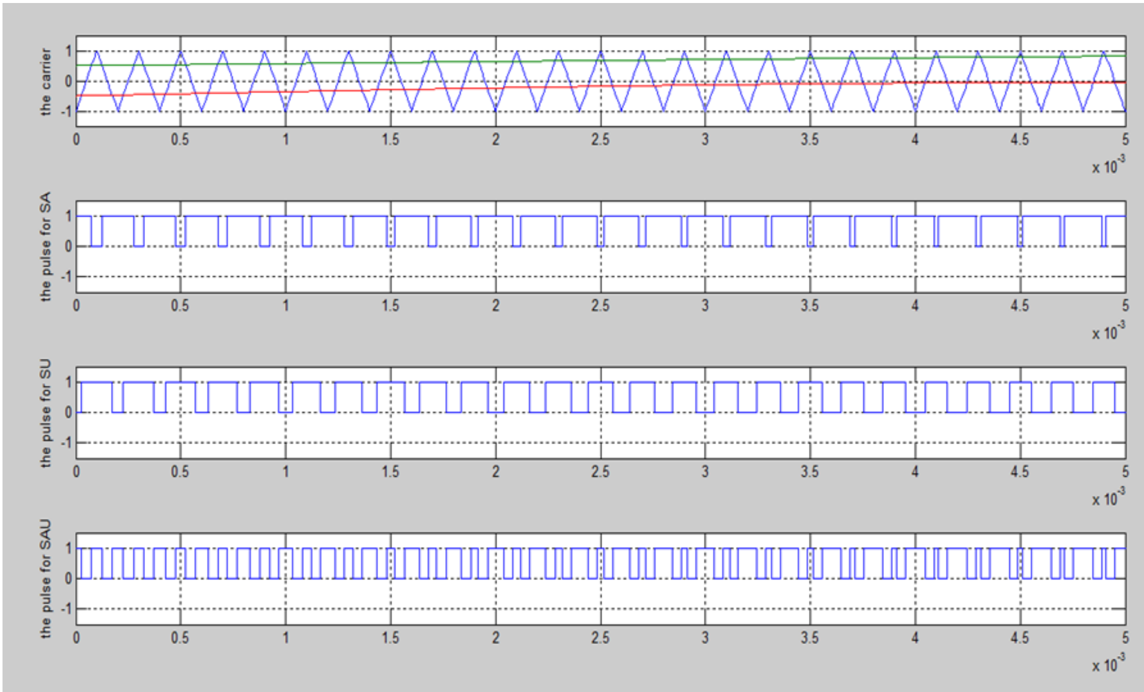

Figure 2.11:The carrier signal, the two reference signals and the gate pulses for switches SA, SU and SAU.

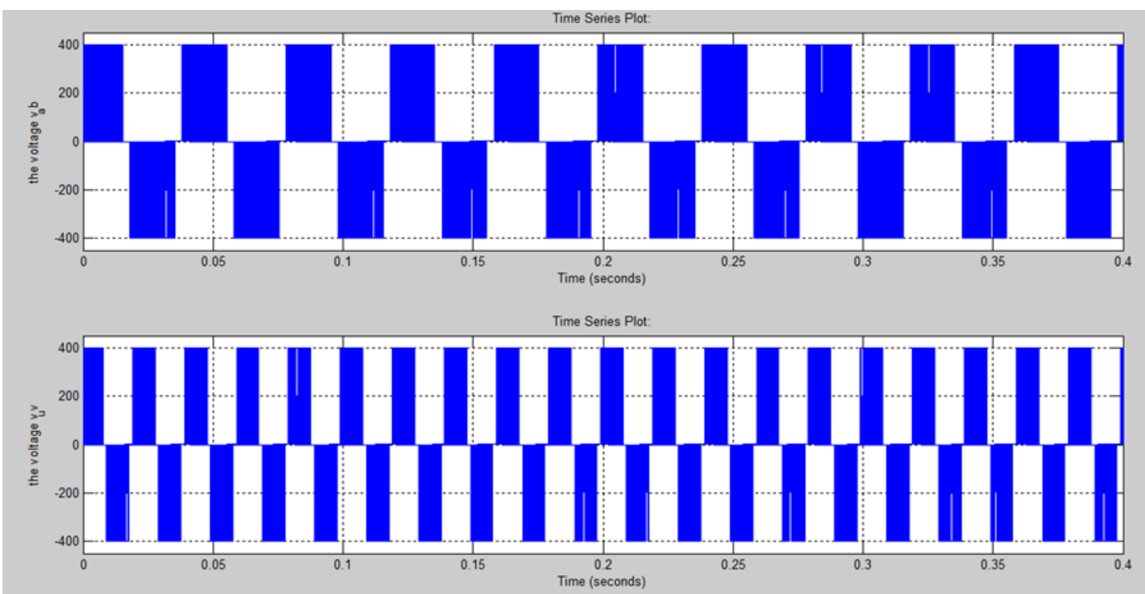

Figure 2.12:The line to line voltages VAB and VUV

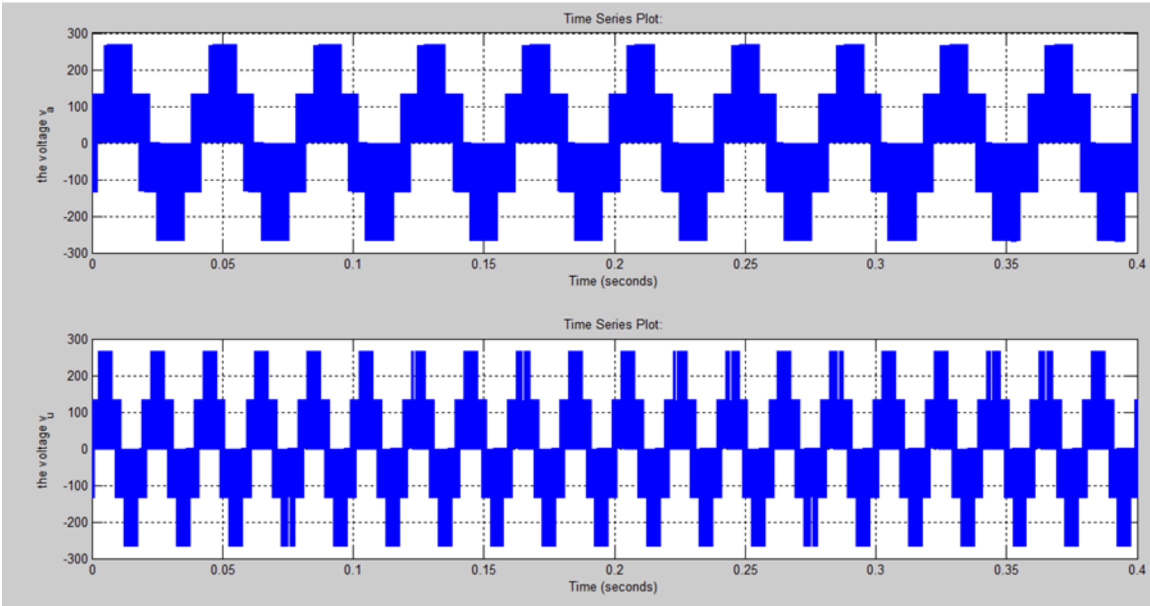

Figure 2.13:The phase voltages VA and VU

2.5.3 Discussion

Figure 2.13 illustrates the SPWM technique for NSI, at any instant two switches are turned on (gate pulse at level 1) and the third switch is off (gate pulse at level 0), the middle switch gating is the logical XOR of the upper and lower gate pulses and at any time, it is impossible to establish a shirt circuit across the supply due to the presence of the XOR gate that generates high logic level only when its inputs are at different logic levels.

Figure 2.14 shows the line to line voltages VAB and VUV , the two signals have two levels +Vdc/-Vdc the frequency of the second signal is double of that of the first signal, this is due to the fact that the lower reference signal's frequency is double of that of the upper one .As a result, the frequency of the output signal is imposed by the frequency of the reference signal.

Figure 2.15 presents the phase voltages the same features exhibited by the line voltages hold for the phase voltages except that the phase voltages have three levels which are 0, (+/-) Vdc/3 and (+/-)2Vdc/3.

2.6 Conclusion

This chapter discussed the operation principle of the three-phase inverter and the nine-switch inverter as well, with the major focus devoted to the NSI, including two modulation techniques that can be applied (SPWM, SVPWM). The first technique was used to develop a MATLAB simulation to validate the performance characteristics and independency in driving two connected loads.

Chapter Three

Application of Vector Control

Chapter 3: Application of Vector control

3.1 Introduction

The control of induction motor can be achieved in two methods scalar control method and vector control method, the first method regards just the steady state model of the motor therefore, the controller cannot give the best performance under the transient state. However, the second method uses a motor model that can achieve good performance in both steady state and transient state [9].In this control technique both the magnitude and the phase of the air gap flux are controlled which provide more precise torque and flux control compared to scalar control, employing this method it is possible to decouple between the control of the flux and the torque similar to the separately excited dc motor, This independent control of flux and torque cannot be reached using scalar control.

This chapter studies the Field oriented control technique, with the major focus given to the indirect rotor field oriented control. First the technique is discussed for a single induction motor, then the same principle is used to control two induction motors powered by NSI. Numerical simulation using MATLAB software with the corresponding results and discussion is undertaken to check its feasibility.

The FOC is achieved in the synchronously rotating dq frame, because the three phase balanced quantities appear as DC quantities [10] [11], this is the starting point if the induction motor is to be controlled like the separately excited DC motor where flux and torque are orthogonal and can be controlled independently.

In electro-mechanical systems torque is the most important variable. It is the link between the mechanical and electrical parts. The following equations represent the torque equation written in the 3-phase system as well as in the dq rotating frame:

$$T_e = \frac{3}{2}\frac{P}{2}\frac{L_m}{L_r}(\phi_r \times I_s) \tag{3.1}$$

$$T_e = \frac{3}{2}\frac{P}{2}(\phi_s \times I_s) \tag{3.2}$$

$$T_e = \frac{3}{2}\frac{P}{2}\frac{L_m}{L_r}\left(i_{qs}\phi_{dr} - i_{ds}\phi_{qr}\right) \tag{3.3}$$

$$T_e = \frac{3}{2}\frac{P}{2}\left(i_{qs}\phi_{ds} - i_{ds}\phi_{qs}\right) \tag{3.4}$$

Compared with a separately excited DC motor torque equation:

$$T_e = k(\phi_f \times I_a) = k'(I_f \times I_a) \tag{3.5}$$

The independent control of the torque and flux is always possible since, the flux and armature current are always perpendicular, the flux is controlled by varying the field current and the torque can be varied by changing the armature current, one can notice that if the angle between the rotor flux and stator current or stator flux and stator current is forced to be 90°, the same principle can be employed to control the induction motor.

The field oriented technique uses this philosophy to achieve the independent control of flux and torque through orientation (alignment) of rotating dq frame , if the second term in equation (3.3) is made to be null the torque equation will seem exactly as the one of the dc motor, this can be realized by orienting the d component of the dq rotating frame toward the rotor or stator flux phasor. Depending to which flux phasor the d component is oriented two types of controllers can be distinguished:

Rotor field-oriented controller (RFOC): when the direct component of the rotating frame is oriented toward the rotor flux vector.

Stator field-oriented controller (SFOC): when the direct component of the rotating frame is oriented toward the stator flux vector.

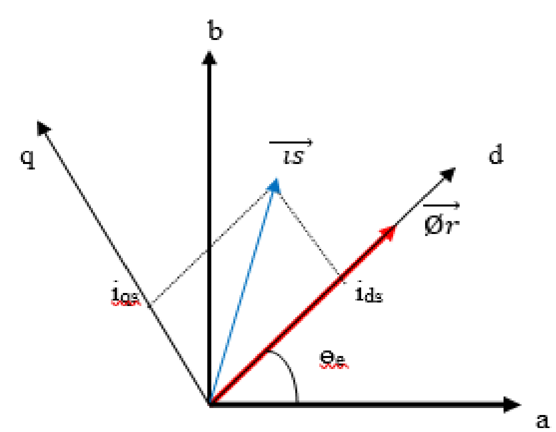

Figure 3.1:Rotor field orientation.

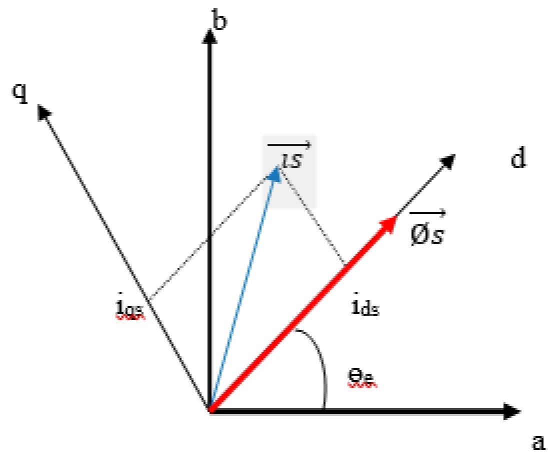

Figure 3.2:Stator flux orientation.

The effect of field oriented control on the torque equation is described by :

$$T_e = \frac{3}{2}\frac{P}{2}\frac{L_m}{L_r}\left(i_{qs}\phi_{dr}\right) = \frac{3}{2}\frac{P}{2}\frac{{L_m}^2}{L_r}\left(i_{qs}i_{ds}\right) \tag{3.6}$$

$$T_e = \frac{3}{2}\frac{P}{2}\left(i_{qs}\phi_{ds}\right) \tag{3.7}$$

The above equation looks pretty similar to that of the DC motor, with:

i_{ds} is the flux producing component and i_{qs} is the torque producing component, figure 3.3 summarizes this information.

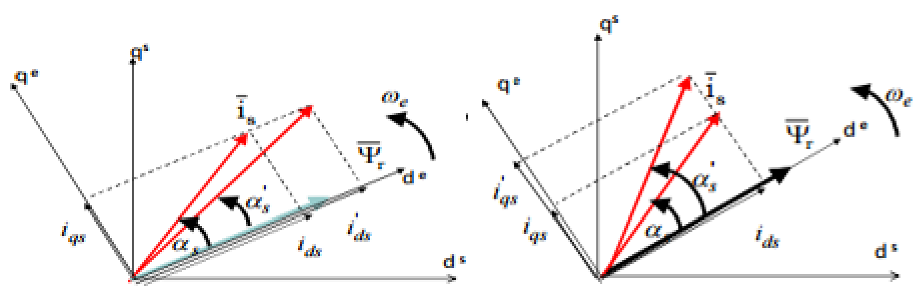

a- i_{qs} is kept constant and i_{ds} is varied to vary the flux.

b- i_{ds} is kept constant and i_{qs} is varied to vary the torque

Figure 3.3:The RFOC and the effect of varying ids and iqs on the flux and torque.

Neglecting the rotor leakage reactance figure 3.4 shows the equivalent circuit of the induction motor when RFOC is applied.

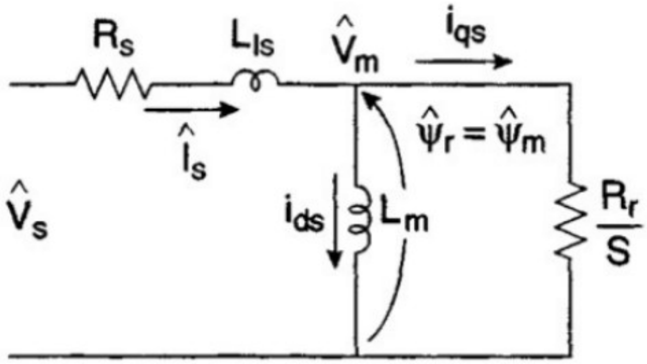

Figure 3.4:Equivalent circuit of induction motor.

The rotor flux phasor and the dq rotating frame rotate at synchronous speed ws , hence the required transformation(orientation) angle qe is obtained by integrating ws . The method used to find the speed ws determines the type of the RFOC:

a- Indirect Rotor Flux Orientation: when the speed ws is found by adding the electrical rotor speed to the slip speed.

b- Direct Flux Orientation: here the orientation angle is found by measurements of the oriented flux components (sensors are required to be installed inside the machine).

3.2 IRFOC:

3.2.1 Modeling of the induction motor under IRFOC

The typical starting point for a derivation of the vector control algorithm is a generalized d q axis dynamic model of the induction motor in a synchronously rotating frame of reference, where the slotting effects, magnetic saturation and eddy current and hysteresis are ignored as are the harmonics of the voltage source.

This model is shown below:

$$\begin{bmatrix} v_{ds} \\ v_{qs} \\ 0 \\ 0 \end{bmatrix} = \begin{bmatrix} R_S + p\sigma L_S & -\omega_e \sigma L_S & p\dfrac{L_m}{L_r} & -\omega_e \dfrac{L_m}{L_r} \\ \omega_e \sigma L_S & R_S + p\sigma L_S & \omega_e \dfrac{L_m}{L_r} & p\dfrac{L_m}{L_r} \\ -\dfrac{L_m}{T_r} & 0 & \dfrac{1}{T_r} + p & -\omega_{sl} \\ 0 & -\dfrac{L_m}{T_r} & -\omega_{sl} & \dfrac{1}{T_r} + p \end{bmatrix} \begin{bmatrix} i_{ds} \\ i_{qs} \\ \phi_{dr} \\ \phi_{qr} \end{bmatrix}$$

Where:

$\sigma = 1 - \frac{{L_m}^2}{L_s L_r}$ is the total leakage factor.

$T_r = \frac{L_r}{R_r}$ is the rotor time-constant.

$\omega_{sl} = \omega_e - \omega_r$ is the slip speed and p is the derivative operator.

The vector controller receives flux and torque commands to generate the dq components of the stator current and the slip speed references. [4].

Under IRFOC

$$\phi_{dr} = |\phi_r| \qquad \phi_{qr} = 0 \tag{3.8}$$

and

$$T_e = \frac{3}{2}\frac{P}{2}\frac{L_m}{L_r}\left(i_{qs}\phi_{dr}\right) = \frac{3}{2}\frac{P}{2}\frac{L_m^2}{L_r}\left(i_{qs}i_{ds}\right) \tag{3.9}$$

It can be easily shown that $\phi_{dr} = L_m i_{ds}$ to derive the equation relating the torque and the components of the stator current:

$$\phi_{dr} = L_r i_{dr} + L_m i_{ds} \tag{3.10}$$

$$v_{dr} = 0 = R_r i_{dr} - (\omega_e - \omega_r)\,\phi_{qr} \tag{3.11}$$

$$\Longrightarrow i_{dr} = 0 \tag{3.12}$$

Now, it is clear that $\phi_{dr} = L_m i_{ds}$ (3.13)

After the application of the IRFOC, the model of the induction motor can be written as:

$$\begin{bmatrix} v_{ds} \\ v_{qs} \\ 0 \\ 0 \end{bmatrix} = \begin{bmatrix} R_S + p\sigma L_S & -\omega_e \sigma L_S & p\frac{L_m}{L_r} & -\omega_e \frac{L_m}{L_r} \\ \omega_e \sigma L_S & R_S + p\sigma L_S & \omega_e \frac{L_m}{L_r} & p\frac{L_m}{L_r} \\ -\frac{L_m}{T_r} & 0 & \frac{1}{T_r} + p & -\omega_{sl} \\ 0 & -\frac{L_m}{T_r} & -\omega_{sl} & \frac{1}{T_r} + p \end{bmatrix} \begin{bmatrix} i_{ds} \\ i_{qs} \\ \phi_r \\ 0 \end{bmatrix}$$

The above model is used to derive the governing equations of the IRFOC, noting that the controller is designed in the dq-rotating frame, starting from the third row:

$$-\frac{L_m}{T_r} i_{ds} + \frac{\emptyset_r}{T_r} + \frac{d}{dt}\phi_r = 0 \tag{3.14}$$

Since $\phi_r = constant$ (3.15)

$$\Longrightarrow i_{ds}{}^* = \frac{1}{L_m}\phi_r{}^* \tag{3.16}$$

From the torque equation (3.9), the quadrature component of the stator current can be deduced:

$$i_{qs}{}^* = \frac{4L_r}{3PL_m}\frac{T_e{}^*}{\phi_r{}^*} \tag{3.17}$$

Considering the fourth row of the above model

$$-\frac{L_m}{T_r} i_{qs} + \omega_{sl}\phi_r = 0 \tag{3.18}$$

$$\Longrightarrow \omega_{sl}{}^* = \frac{L_m}{T_r}\frac{i_{qs}{}^*}{\phi_r{}^*} \tag{3.19}$$

The transformation angle is required, since the three phase quantities are needed by the inverter, this angle can be obtained as follow

$$\theta_e{}^* = \int (\omega_r + \omega_{sl}{}^*)\, dt \tag{3.20}$$

The above equations are enough if a current controlled inverter is used.

For a voltage controlled inverter the equations of the stator voltage must be used, these equations can be deduced from the first and second row of the model subjected to IRFOC [12],

$$v_{ds} = R_s i_{ds} + \sigma L_s \frac{d}{dt} i_{ds} - \omega_e \sigma L_s i_{qs} \tag{3.21}$$

$$v_{qs} = \omega_e \sigma L_s i_{ds} + R_s i_{qs} + \sigma L_s \frac{d}{dt} i_{qs} + \omega_e \frac{L_m}{L_r} \phi_{dr} \tag{3.22}$$

It can be remarked that both direct and transverse component of stator current appear at the same time in the expression of v_{ds} and v_{qs} thus, it is necessary to use decoupling techniques to separate between the d and q components.

3.2.2 Decoupling using compensation:

In the IRFOC scheme, two current regulators are used, one for the d axis and the other for the q axis, to compare between the reference and actual values of the current components to generate the required d and q components of stator voltage, the output of the current regulators is:

$$v_{ds} = (R_s + \sigma p L_s) i_{ds} = {v_{ds}}^* + e_{ds} \quad \text{where} \quad e_{ds} = \omega_e \sigma L_s i_{qs} \tag{3.23}$$

$$v_{qs} = (R_s + \sigma p L_s) i_{qs} = {v_{qs}}^* - e_{qs} \quad \text{where} \quad e_{qs} = \omega_e \sigma L_s i_{ds} + \omega_e \frac{L_m}{L_r} \phi_{dr} \tag{3.24}$$

The terms e_{ds} and $-e_{qs}$ must be added to the output of the PI current regulator to find the dq components of the stator voltage.

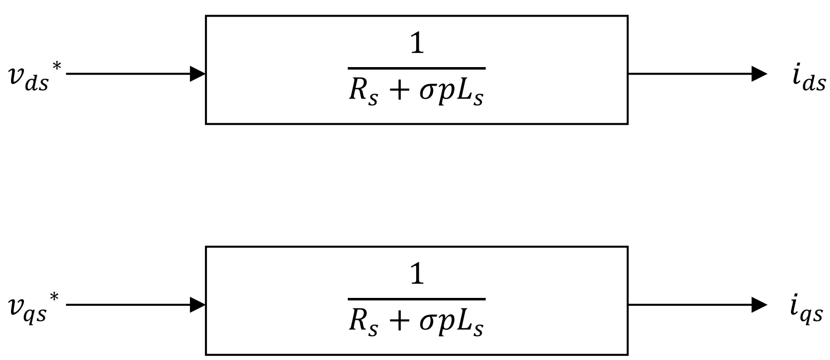

The general block diagram of the IRFOC is shown in figure 3.5:

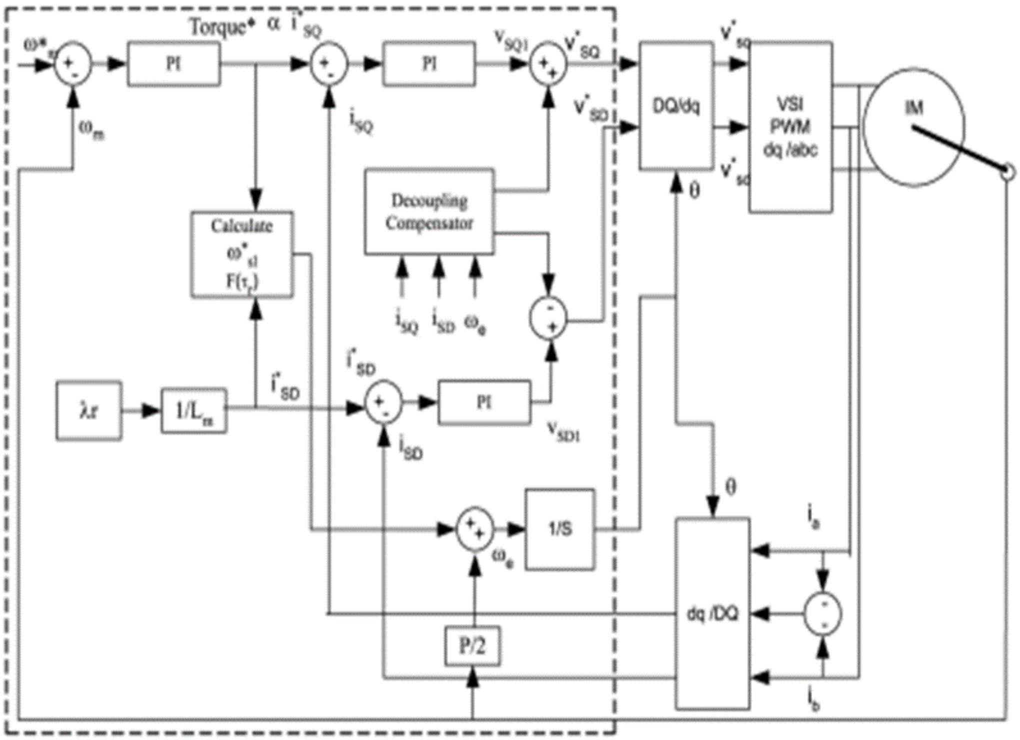

Figure 3.5:General block diagram for the IRFOC technique.

Three PI controllers are used:

d-axis stator current controller

q-axis stator current controller

speed controller whose output is the reference torque being fed to the IRFOC.

The IRFOC outputs the reference values of stator current in the dq frame and the transformation angle $\theta_e{}^*$, for the current to be regulated, the actual d and q component in the induction motor must be obtained, this leads to the application of the Park Transformation to transform the three phase (abc) currents into the two phase synchronously rotating frame(dq).

The PI current controllers compare the actual currents with their reference values and generate the required stator voltages. These voltages are corrected using the decoupling compensator to obtain the required d and q-axis components of the stator reference voltage that must be transformed to the three phase system using Inverse Park Transform. Obtained voltages are fed the inverter with the necessary reference voltages used in obtaining the gating signals of the switches (SPWM).

3.2.3 Speed and current regulators tuning:

3.2.3.1 speed regulator:

*3.2.3.1.1 P*I controller:

The PI parameters are obtained based on the block diagram represented in figure 3.6.

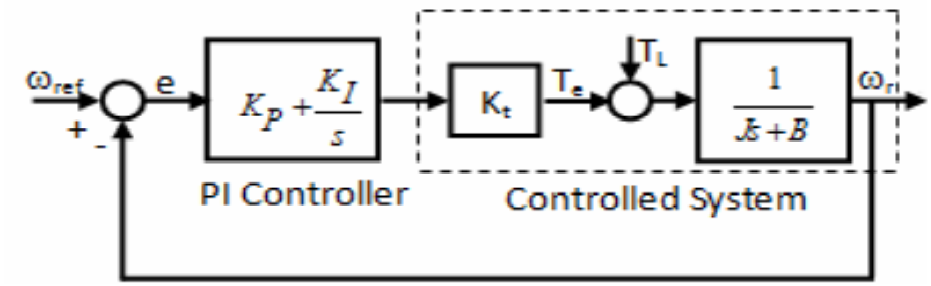

Figure 3.6:Simplified model of the IM drive with PI controller .

Where ω*r*ef is the reference rotor angular speed, ω*r* is the rotor angular speed, *e*=ω*ref*-ω*r* is the tracking speed error, KP is the proportional gain, KI is the integral gain, *B* is the total damping coefficient, and *Te* denotes the electromagnetic torque. The *Te* can be defined as

$$T_e = K_t * i_{qs} = \frac{3}{2}\frac{P}{2}\frac{L_m^2}{L_r}\left(i_{qs}i_{ds}\right) \tag{3.25}$$

where *i*qs and *i*ds denote the torque and flux current commands, respectively. If TL=0, the closed loop transfer function is as follows:

$$\frac{\omega r}{\omega ref} = \frac{K_t(K_I + K_p s)}{Js^2 + \left(B + K_p K_t\right)s + K_I K_t} \tag{3.26}$$

3.2.3.1.2 IP controller:

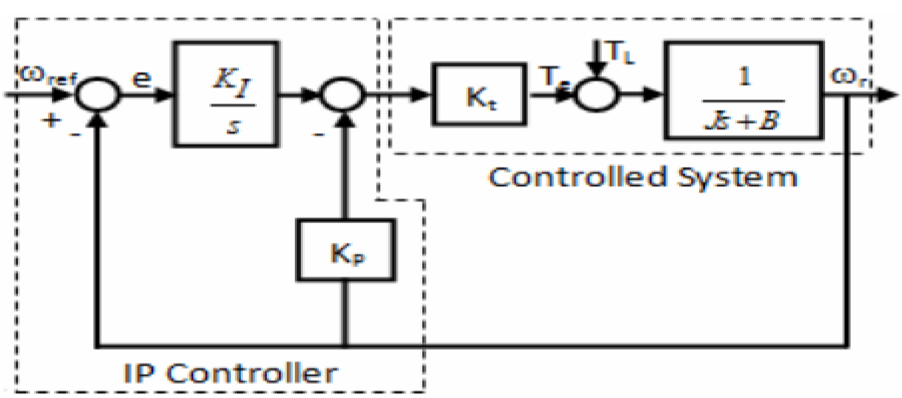

Figure 3.7:Simplified model of the IM drive with IP controller.

To improve the dynamic performance for transient state and avoid overshoot, the speed control is confided to an integral plus proportional controller [13]. The IP controller is considered the major contribution in this project. Figure above shows the Simplified block diagram of the speed control of induction motor using the integral plus proportional controller.

It has some clear differences with PI controller. If *TL=0*, the closed loop transfer function will become:

$$\frac{\omega r}{\omega ref} = \frac{K_t K_I}{Js^2 + (B + K_p K_t)s + K_I K_t} \tag{3.27}$$

3.2.3.2 Current regulators:

3.2.3.2.1 d-axis current regulator

It provides the V_{ds} component as explained before, its parameters can be found using the loop shown in figure 3.5.

The transfer function of the i_{ds} regulator is given by: $C_i(s) = K_{pi} + \frac{K_{ii}}{s}$ (3.28)

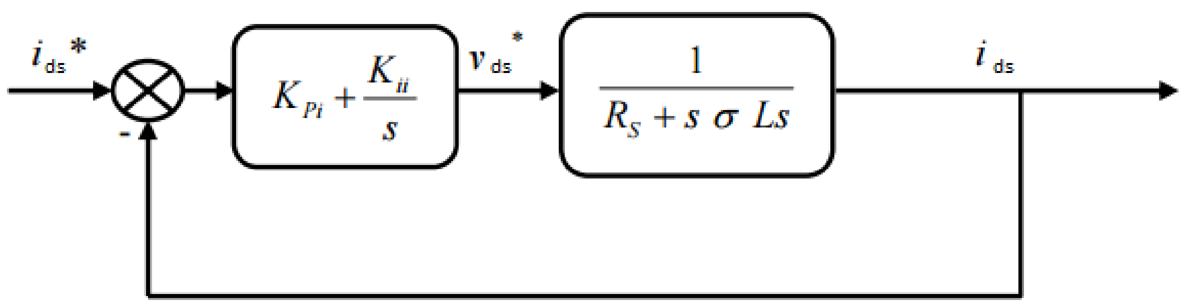

Figure 3.8:The d-axis current loop

The open loop transfer function is:

$$H(s) = K_{pi}\left(s + \frac{K_{ii}}{K_{pi}}\right)\frac{1}{s}\frac{\frac{1}{\sigma L_s}}{\frac{R_s}{\sigma L_s} + s} \tag{3.29}$$

Using pole/zero cancelation by setting $\frac{K_{ii}}{K_{pi}} = \frac{R_s}{\sigma L_s}$, H(s) reduces to:

$$H(s) = \frac{K_{pi}}{s}\frac{1}{\sigma L_s} \tag{3.30}$$

Thus, the closed loop transfer function is written as:

$$G(s) = \frac{H(s)}{1 + H(s)} = \frac{\frac{K_{pi}}{s}\frac{1}{\sigma L_s}}{1 + \frac{K_{pi}}{s}\frac{1}{\sigma L_s}} = \frac{1}{\frac{\sigma L_s}{K_{pi}}s + 1} = \frac{1}{\tau s + 1} \tag{3.31}$$

With: $\tau = \frac{\sigma L_s}{K_{pi}}$, the gains of the d-axis current regulator can be obtained for a given value of τ.

3.2.3.2.2 q-axis current regulator

Proceeding the same way, the gains of the i_{qs} regulator can be determined using the same loop with the d subscript being replaced by the q subscript to indicate the q axis.

3.3 IRFOC of two motors fed by nine switch inverter

The technique of IRFOC was applied to a single induction motor however, the same principle is used to drive two motors powered by a nine-switch inverter based on the IRFOC of each IM alone. The figure 3.5 summarizes the structure of this technique.

The control scheme proposed in figure 3.9 is valid for nine switch inverter, one IRFOC is used to generate the reference voltages for the upper switches and another IRFOC provides the reference signals to the bottom switches, the gate signals for the middle switches is the logical XORing of the upper and lower gate signals as discussed in chapter 2.

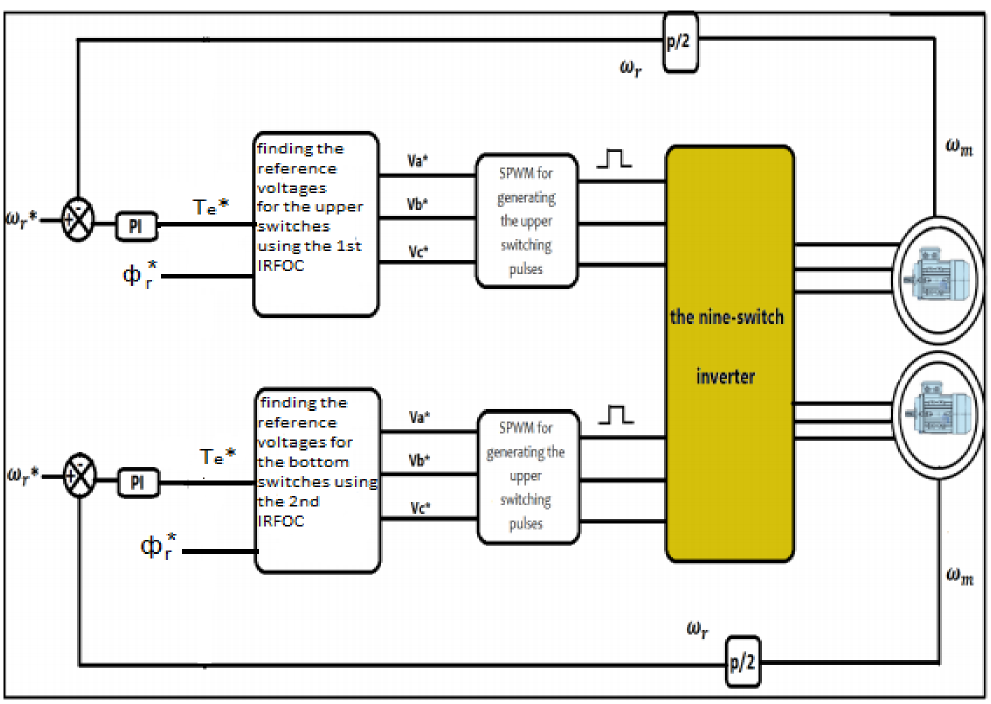

Figure 3.9:The general block diagram of vector control of nine switch inverter driving two induction motors

3.4 Simulation Results and Analysis:

In this chapter the MATLAB/SIMULINK simulation and results of vector control (IRFOC) of the nine-switch inverter fed induction motor are presented. The motors used in this simulation are identical and their rated voltage, power, rated speed, number of poles and frequency are respectively: 400V, 3hp, 1500 rpm, 4 poles and 50Hz.

3.5 IRFOC of two induction motors using MATLAB/SIMULINK

The block diagram of figure 3.10 shows the IRFOC technique applied to the nine-switch inverter fed motors. During this simulation the reference flux is set at 1.1 Wb for each motor and the speed references are selected to be 60 rad/s for the upper motor and 70 rad/s for the lower motor. The load torque of 10 N.M is introduced to the first motor at the instant t=3 sec, and the second motor is loaded with a torque of 5 N.M at the instant t=3.5 sec, after that the speed commands for motor1 and motor2 are respectively changed to -60 rad/s at t=3 sec,-70 rad/s at t=5 sec and the mechanical speeds, electromagnetic torques and stator currents are measured.

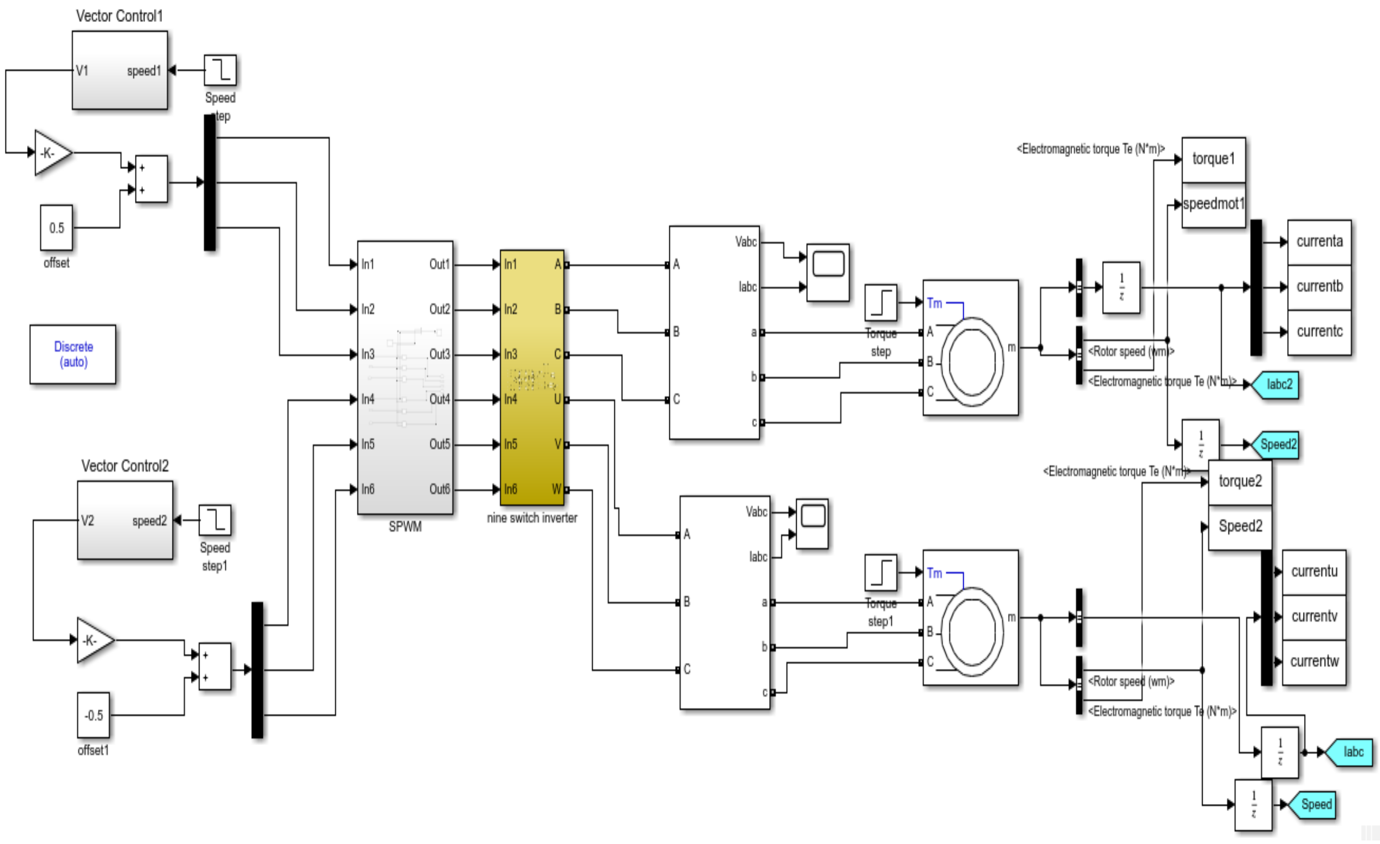

Figure 3.10:Simulink model of two induction motor fed by nine switch inverter.

3.5.1 Simulation Results:

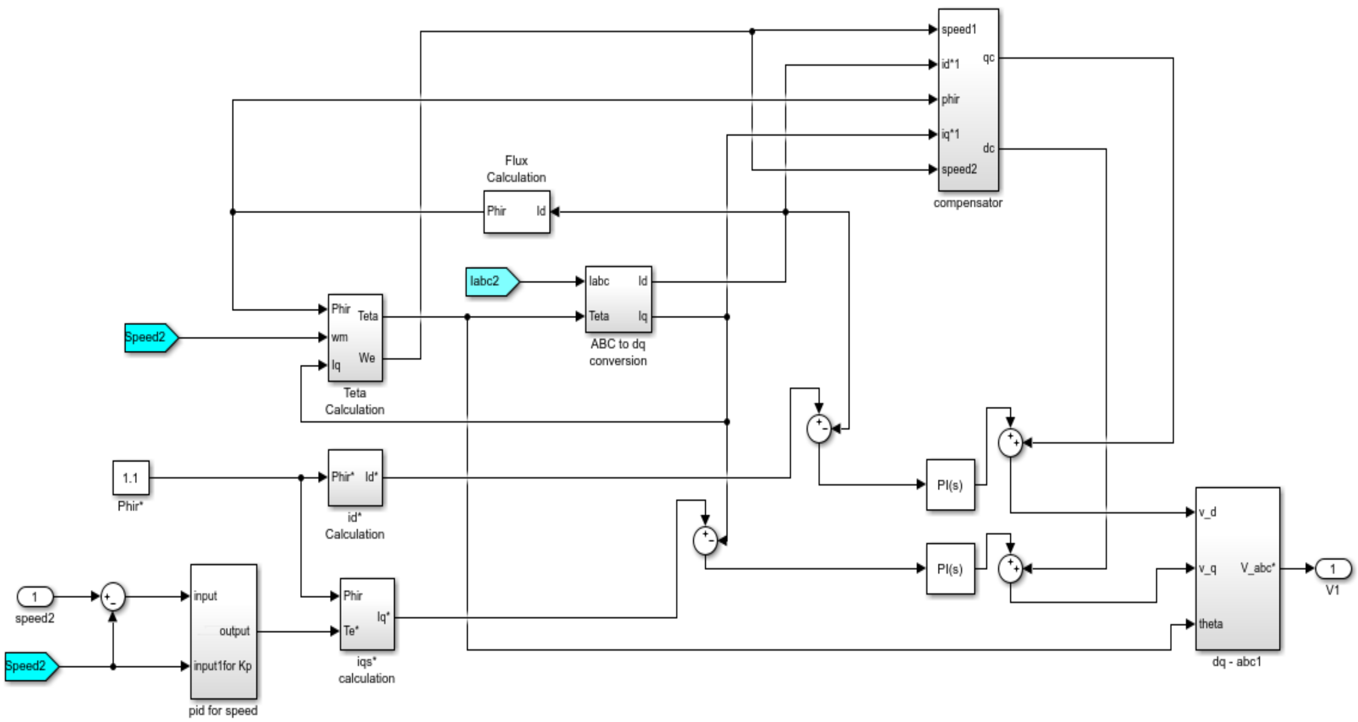

Figure 3.11:IRFOC SIMULINK block diagram for the upper motor.

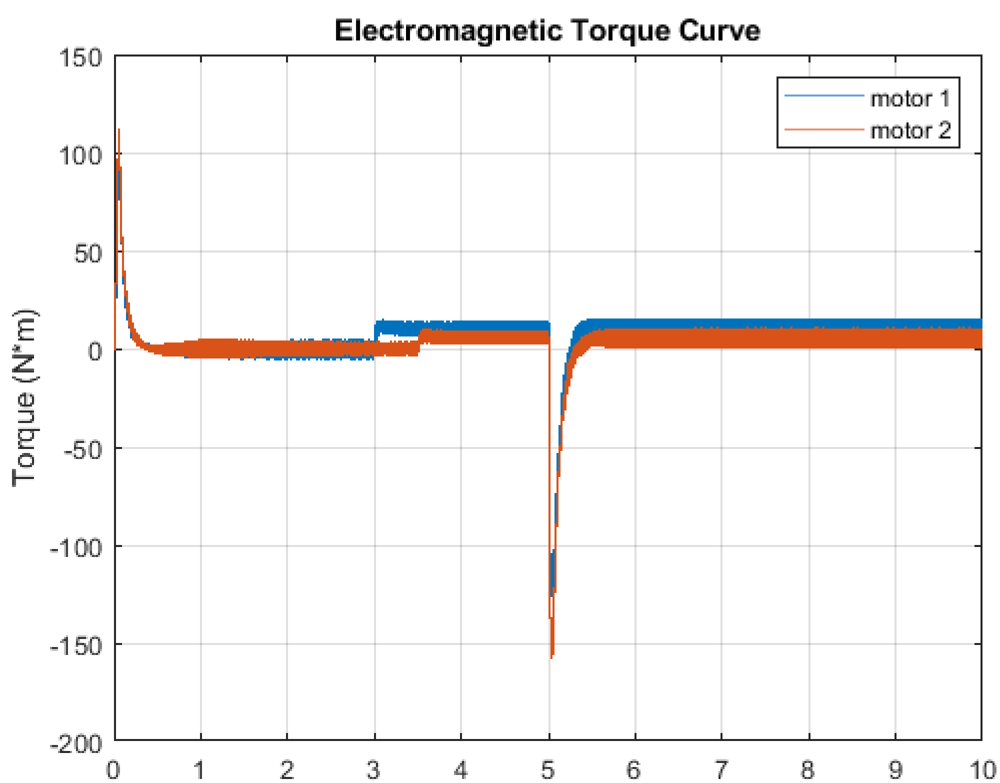

Figure 3.12: Electromagnetic torque curve.

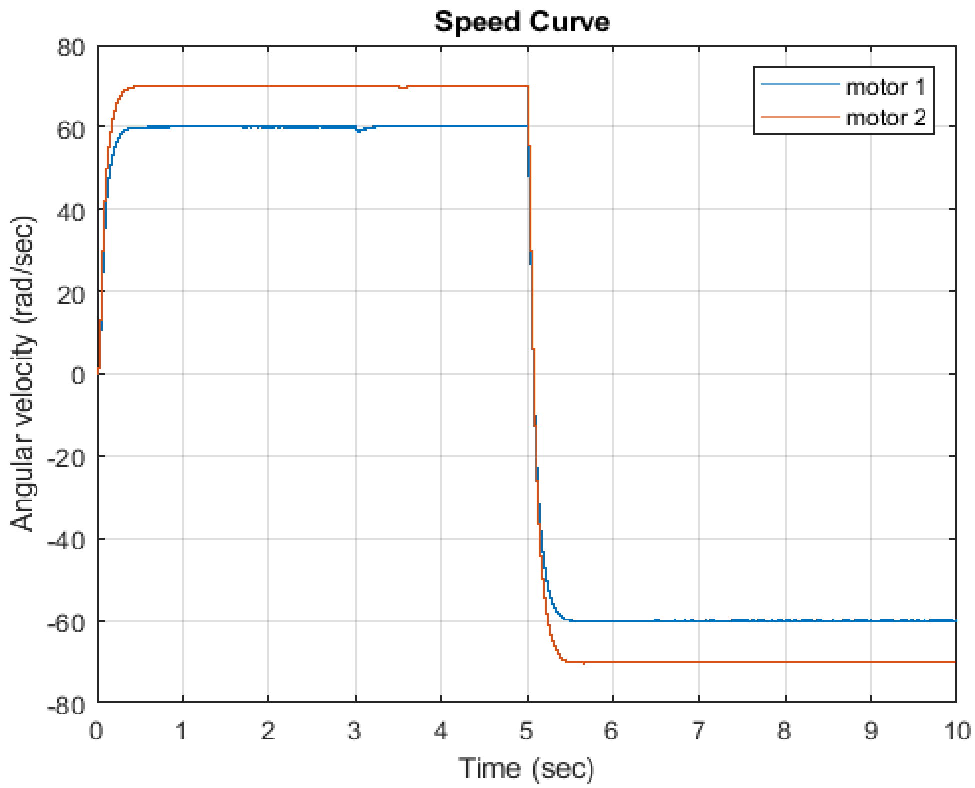

Figure 3.13: Angular velocity of the two induction motors.

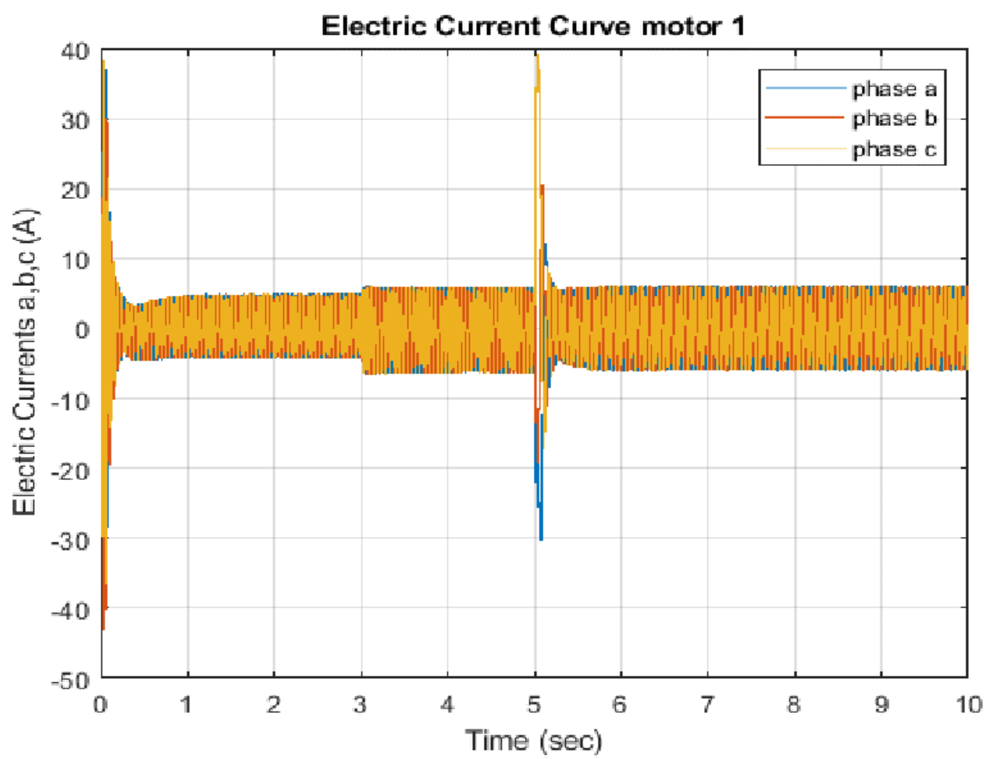

Figure 3.14: Electric current curve versus time for motor 1

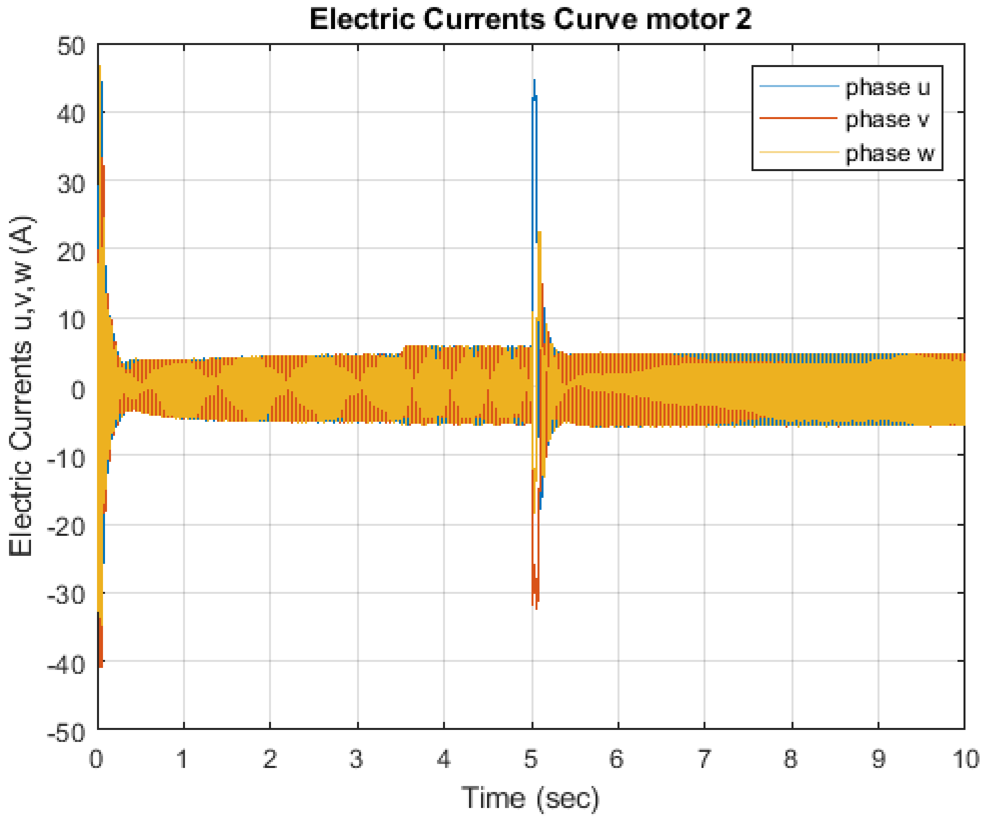

Figure 3.14:Electric current versus time for motor 2.

3.6 Discussion:

The above figures represent the simulation results obtained for a simulation time of 10 sec.

Figure 3.12 shows the torque response of the two motors, a high starting torque can be noticed which is one of the characteristics of the induction motors, the torque values drop and settle at zero, when the load torques are introduced the torque values increase to meet the load requirements (to balance the loads), when the sign of the speed reference is reversed the torque decreases to reach negative values due to the large negative mismatch between the reference speed imposed by the controller and the actual speed of the motor, the speed regulator processes this error and gradually reduces it to small values, as a results the torque increases and return back to its previous value.

Figure 3.13 represents the speed response of the two motors, before introducing the loads, the motors follow exactly their reference speeds as the load torques are zero, that is, there are no opposing torques that contribute to damp the motors motion. When the load torques are added the speeds drop as a response to the damping exerted by the load torques, after small amount of time the speeds increase and return back to their reference values due to the speed compensation offered by the speed controllers(PIs make the error between the reference and measured speeds as small as possible). When the sign of the speed references are reversed the motors exhibit the same features.

Figures 3.14 and 3.15 illustrate the stator current profiles of motor1 and motor2, at starting the motors draw very high currents which are needed to set up the revolving magnetic fields in the air gaps, after small amount of time the currents settle at small values because at no load the slip value is very close to zero which results in high impedance value seen by the stator this definitely results in small currents , when the torque is applied more currents are drawn because the slip increases resulting in a decrease in the impedance value thus the currents increase.

3.7 Conclusion:

In this chapter the principle of the vector control technique was explained, the IRFOC technique was the main scope of this chapter, it was generally discussed for a single induction motor then specifically studied for the nine-switch inverter fed induction motors. Finally, the MATLAB simulation blocks stamped with the results of simulation and discussion were presented. The simulation results succeed to prove the independent control of the two driven motors, and the effectiveness of the IRFOC technique in achieving good quality performance of the driven loads.

Chapter Four

Application of Direct Torque Control

Chapter 4: Application of Direct Torque Control

4.1 Introduction

Advanced control of electrical machines requires an independent control of magnetic flux and torque. For that reason, it was not surprising that the DC machine played an important role in the early days of high-performance electrical drive systems, since the magnetic flux and torque are easily controlled by the stator and rotor current, respectively. The introduction of field-oriented control meant a huge turn in the field of electrical drives, since with this type of control the robust induction machine can be controlled with a high performance. Later in the 1980s, a new control method for induction machines was introduced: The direct torque control (DTC) method. It was proposed by Takahashi and Depenbrock [14] [15] . It based on the direct selecting of the switching states to control the voltage source inverter (VSI) through a switching look-up table.

The aim of this chapter is to design and modeling the direct torque control (DTC) of induction motor (IM). The first method is a conventional direct torque control (C-DTC) where the torque and the flux are regulated by the hysteresis controllers.

4.2 Model of induction motor dedicated for direct torque control

The mathematical model of induction motor can be described in the stator fixed reference frame (α, β) (stationary frame) by assuming the rotor and the stator flux as state variable.

$$\frac{dX}{dt} = AX + BU$$

With

$$X = \begin{bmatrix} \phi_{s\alpha} \\ \phi_{s\beta} \\ \phi_{r\alpha} \\ \phi_{r\beta} \end{bmatrix}, A = \begin{bmatrix} \frac{R_s}{\sigma L_s} & 0 & \frac{L_m R_s}{L_r L_s} & 0 \\ 0 & \frac{-R_s}{\sigma L_s} & 0 & \frac{L_m R_s}{\sigma L_r L_s} \\ \frac{L_m R_r}{\sigma L_r L_s} & 0 & \frac{-R_r}{\sigma L_r} & -\omega \\ 0 & \frac{L_m R_r}{\sigma L_r L_s} & \omega & \frac{-R_r}{\sigma L_r} \end{bmatrix}, B = \begin{bmatrix} 1 & 0 \\ 0 & 1 \\ 0 & 0 \\ 0 & 0 \end{bmatrix}, \ U = \begin{bmatrix} \vartheta_{s\alpha} \\ \vartheta_{s\beta} \end{bmatrix}$$

Where

$\phi_{s\alpha}, \phi_{s\beta}, \phi_{r\alpha}, \phi_{r\beta}$ are stator and rotor flux components.

R_s, R_r are stator and rotor resistance.

$L_{r,} L_s$ are stator and rotor inductance.

L_m is the mutual stator-rotor inductance.

$\sigma = 1 - \frac{L_m{}^2}{L_r L_s}$is the Blondel's coefficient and ω is the machine speed ($\omega = p\Omega = \omega s$- ωr and p is the pole pair number).

The rotor motion can be described by:

$$J\frac{d\Omega}{dt} = T_{em} - T_L - f\Omega \tag{4.1}$$

where J is the motor inertia, T_{em} is the electromagnetic torque, T_L is the load torque, and f is the friction coefficient.

4.3 Principles of direct torque control

Direct torque control principle was introduced in the late 1980s by [14] [15]. It achieves a decoupled control of the stator flux and the electromagnetic torque in the stationary frame (α, β), and it allows induction machines to have an accurate and fast electromagnetic torque response. It uses a switching table for the selection of an appropriate voltage vector. The selection of the switching states is related directly to the variation of the stator flux and the torque of the machine. Hence, the selection is made by restricting the flux and torque magnitudes within two hysteresis bands. Those controllers ensure a separate regulation of both of these quantities [16] [17] [18] .The inputs of hysteresis controllers are the flux and the torque errors as well as their outputs determine the appropriate voltage vector for each commutation period.

4.4 Estimation of stator flux and electromagnetic torque

4.4.1 Control of stator flux

Based on the induction motor model in stationary frame, the stator flux equation can be expressed as follows [19] [20] [21] [22] [23]:

$$\phi_{s\alpha} = \int (v_{s\alpha} - R_s i_{s\alpha}) dt \tag{4.2}$$

$$\phi_{s\beta} = \int \left(v_{s\beta} - R_s i_{s\beta}\right) dt \tag{4.3}$$

Considering that the control of the switches of the inverter is done by control period (or sampling) T_s and that at each of these periods the states Sa, Sb, and Sc are kept constant, the method of numerical integration of the rectangles makes it possible to obtain an expression of the sample *k + 1* of the stator flux in the following form [24]:

$$\phi_{s\alpha}(k+1) = \phi_{s\alpha}(k) + \big(v_{s\alpha}(k) - R_s i_{s\alpha}(k)\big)T_s \tag{4.4}$$

$$\phi_{s\beta}(k+1) = \phi_{s\beta}(k) + \Big(v_{s\beta}(k) - R_s i_{s\beta}(k)\Big)T_s \tag{4.5}$$

Using phasor form, the above expressions can be written as follows:

$$\overrightarrow{\phi_s}(k+1) = \overrightarrow{\phi_s}(k) + \Big(\vec{V_s}(k) - R_s\vec{I_s}(k)\Big)T_s \tag{4.6}$$

We can neglect the stator resistance voltage drop compared to *Vs* for high speed regions. Then Eq. (4.6) can be written as:

$$\vec{\phi}_s(k+1) = \vec{\phi}_s(k) + \overrightarrow{V_s}(k)T_s \tag{4.7}$$

Eq. (4.7) shows that the stator flux can be changed by the application of stator voltage during time Ts. The stator flux vector's extremity moves in direction given by the voltage vector and making a circular trajectory.

A two-level hysteresis comparator is used for flux regulation. It allows to drop easily the flux vector extremity within the limits of the two concentric circles with close radius. The choice of the hysteresis bandwidth depends on the switching frequency of the inverter.

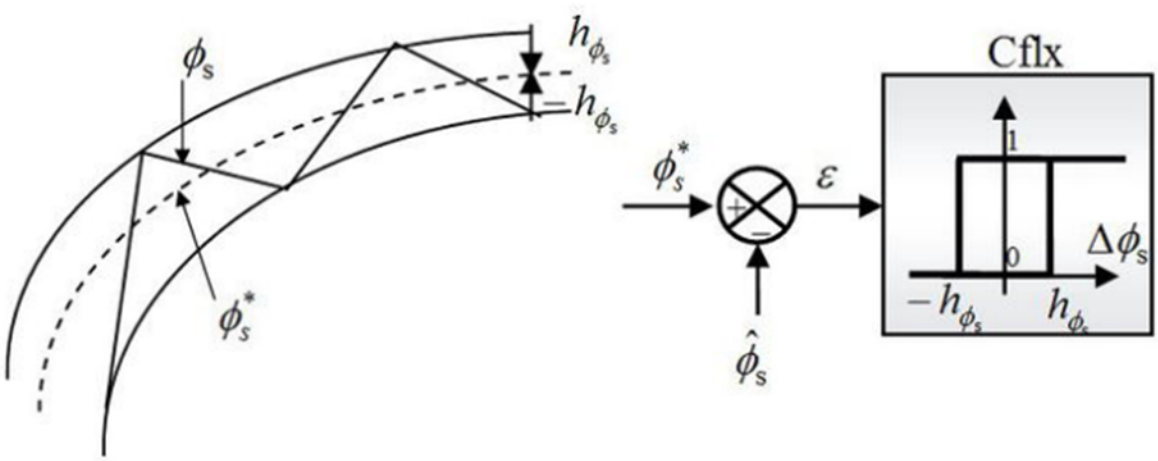

Figure 4.1: Two-level hysteresis comparator for stator flux control.

The logical outputs of the flux controller are defined as:

$$Cflx = 1 \ \ if \Delta\phi_s > h_{\phi s} \tag{4.8}$$

$$Cflx = 0 if \ \ \Delta\phi_s \leq -h_{\phi s} \tag{4.9}$$

where $h_{\phi s}$ is hysteresis band of stator flux.

The stator flux error is defined by the difference between the reference value of flux and the actual estimated value:

$$\Delta\phi_s = |\phi_s^*| - |\phi_s| \tag{4.10}$$

4.4.2 Control of electromagnetic torque

During one sampling period, the rotor flux vector is supposed invariant. The rotor and stator flux vectors are linked by the following relation:

$$\phi_r = \frac{L_m}{L_s} \cdot \frac{\phi_s}{1 + j\sigma\omega T_r} \tag{4.11}$$

The angle between these two vectors is given by:

$$\delta = Arctang(\sigma\omega T_r) \tag{4.12}$$

Finally, between the modulus of the two flux vectors, we have the following relation:

$$|\phi_r| = \frac{L_m}{L_s} \cdot \frac{|\phi_s|}{\sqrt{1 + (\sigma\omega Tr)^2}} \tag{4.13}$$

The general expression of electromagnetic torque is given by:

$$T_e = \frac{3}{2} p \frac{L_m}{\sigma L_s L_r} [\phi_s \phi_r] \tag{4.14}$$

$$T_e = \frac{3}{2} p \frac{L_m}{\sigma L_s L_r} \phi_s \phi_r Sin(\delta) \tag{4.15}$$

where:

p **is** the number of pole pairs**.**

ϕ_s, ϕ_r are stator and rotor flux vectors.

δ is the angle between the stator and rotor flux vectors.

From expression (4.15), it is clear that the electromagnetic torque is controlled by the stator and rotor flux amplitudes. If those quantities are maintaining constant, the torque can be controlled by adjusting the load angle δ.

The torque regulation can be realized using three-level hysteresis comparator and the logical outputs of the torque controller are defined as:

$$Ctrq = 1 \qquad if \Delta T_e > h_{Te} \tag{4.16}$$

$$Ctrq = 0 \qquad if - h_{Te} \leq \Delta T_e \leq h_{Te} \tag{4.17}$$

$$Ctrq = -1 \qquad if \Delta T_e < -h_{Te} \tag{4.18}$$

where h_{Te} is hysteresis band of torque.

The torque error is defined by the difference between the reference's values of the torque and the actual values:

$$\Delta T_e = T_e^* - T_e \tag{4.19}$$

4.5 Estimation of stator flux and electromagnetic torque

4.5.1 Stator flux estimation

The amplitude of the stator flux is estimated from its two-phase components $\phi_{s\alpha}$and $\phi_{s\beta}$:

$$\phi s = \sqrt{\left(\phi_{s\alpha}^2 + \phi_{s\beta}^2\right)} \tag{4.20}$$

The stator voltage components $V_{s\alpha}$ and $V_{s\beta}$ are obtained by applying Concordia transformation on the output voltage of the three-phase VSI which are given by:

$$v_{s\alpha} = \sqrt{\frac{2}{3}} V_{dc} \left[S_a - \frac{1}{2}(S_b + S_c)\right] \tag{4.21}$$

$$v_{s\beta} = \sqrt{\frac{1}{2}} V_{dc} (S_b - S_c) \tag{4.22}$$

The stator currents components $i_{s\alpha}$ and $i_{s\beta}$ can be obtained also by applying Concordia transformation on the measured currents:

$$i_{s\alpha} = \sqrt{\frac{3}{2}} i_{sa} \tag{4.23}$$

$$i_{s\beta} = \frac{1}{\sqrt{2}} (i_{sb} - i_{sc}) \tag{4.24}$$

4.5.2 Electromagnetic torque estimation

The produced electromagnetic torque of the induction motor can be determined using the cross product of the stator quantities (i.e., stator flux and stator currents). The torque formula is expressed as the following:

$$T_e = \frac{3}{2} p\left(\overrightarrow{\phi_s} \text{ X } \vec{\iota_s}\right) \tag{4.25}$$

4.6 Switching table construction and control algorithm design

To maintain a decoupled control, a pair of hysteresis comparators receive the stator flux and torque errors as inputs. Then, the comparators output determines the appropriate voltage vector selection. However, the choice of voltage vector is not only depending on the output of hysteresis controllers but on the position of stator flux vector also. Thus, the circular stator flux vector trajectory will be divided into six symmetrical sectors (Table 4-1).

Table 4-1:Generalized switching table.

	Increases	Decreases
ϕ_s	V_{i-1} and V_{i+1}	V_{i+2} and V_{i-2}
T_{em}	V_{i+1} and V_{i+2}	V_{i-1} and V_{i-2}

For each sector, the vectors ($\mathrm{V_i}$ *and* $\mathrm{V_{3+i}}$) are not considered because both of them can increase or decrease the torque in the same sector according to the position of the flux vector on the first or the second sector.

If the zero vectors V_0 and V_7 are selected, the stator flux will stop moving, its magnitude will not change, and the electromagnetic torque will decrease, but not as much as when the active voltage vectors are selected. The resulting look-up table for DTC which was proposed by Takahashi is presented in Table 2.

Table 4-2:Look-up table for basic direct torque control.

Flux	Torque	1	2	3	4	5	6	Comparator
Cflx=1	Ctrq=1	V_2	V_3	V_4	V_5	V_6	V_1	Two-level
	Ctrq=0	V_7	V_0	V_7	V_0	V_7	V_0	
	Ctrq=-1	V_6	V_1	V_2	V_3	V_4	V_5	Three-level
Cflx=0	Ctrq=1	V_3	V_4	V_5	V_6	V_1	V_2	Two-level
	Ctrq=0	V_0	V_7	V_0	V_7	V_0	V_7	
	Ctrq=-1	V_5	V_6	V_1	V_2	V_3	V_4	Three-level

4.7 Global scheme of direct torque control

The global control scheme of direct torque control strategy is shown in Figure 4.2. It is composed of speed regulation loop; the proportional-integral (PI) controller is used for the regulation. It is performed by comparing the speed reference signal to the actual measured speed value. Then the comparison error becomes the input of the PI controller [25].

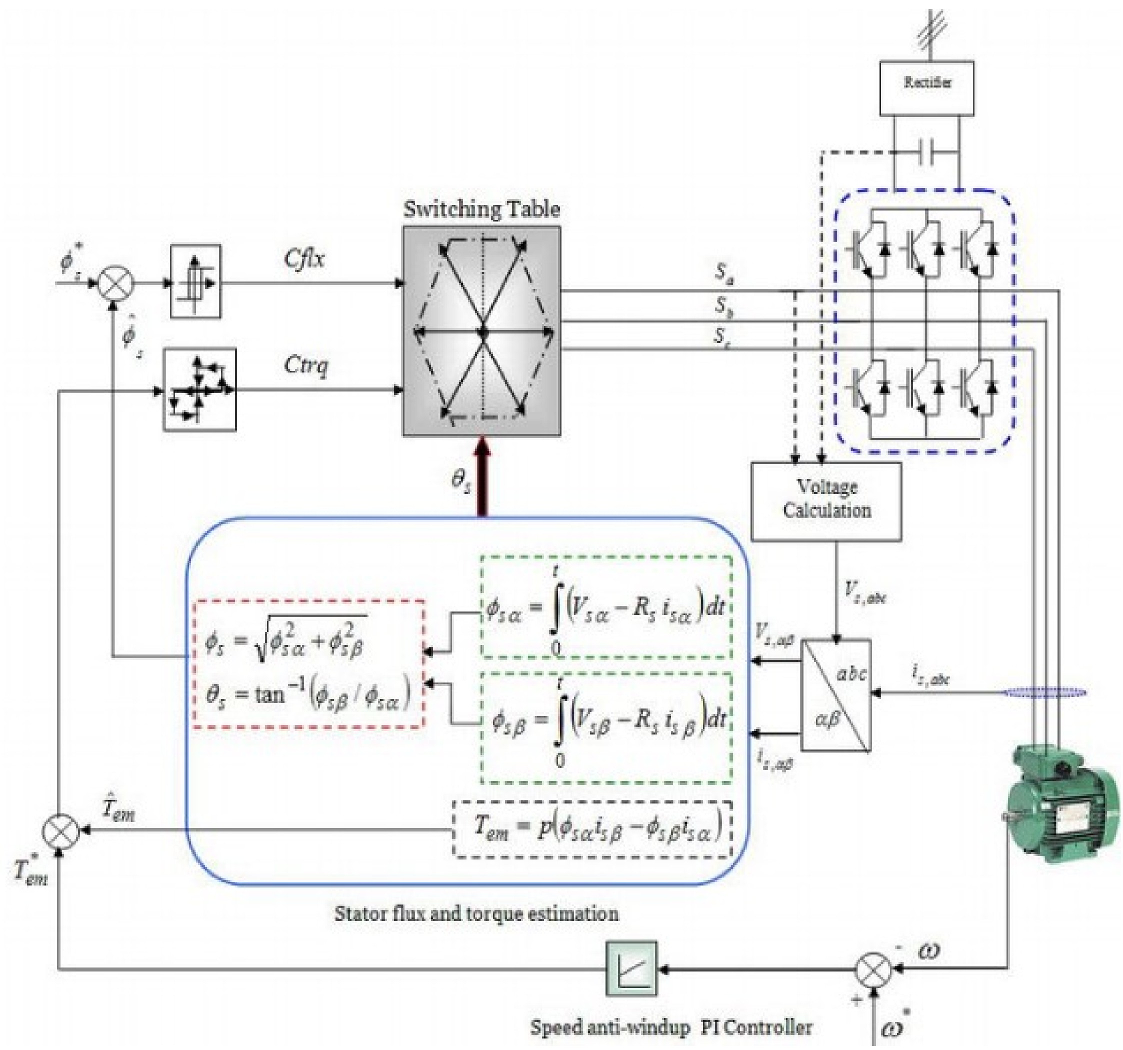

Figure 4.2:Global control scheme of basic direct torque control.

4.8 Space vector modulation of NSI

The NSI can be viewed as two conventional two-level inverters sharing the middle three switches. It is composed of three legs and each leg contains three switches. In each of the three legs and at any given instant, only one switch out of the three is allowed to be open in order to avoid short-circuiting the power supply through the inverter legs and to avoid keeping the loads floating. Consequently, the NSI has 27 possible switching combinations. Each leg can be in three different switch ON-OFF position. These positions are referred as {1}, {0}, and {-1}.

Referring to Table 3 shows all permissible states of the three legs. Due to the aforementioned constraint, only 27 states are allowed and it can be classified in 5 groups [17]:

- **Zero vectors**: Both outputs are in zero state. In zero state, a load is short circuited trough one of the DC rails.
- **Upper active vectors**: Upper output is in active state but lower output is in zero state.
- **Lower active vectors**: Lower output is in active state but upper output is in zero state.
- **Same active vectors**: both outputs are in similar active state.
- **Middle active vectors:** outputs are in different active states (neighbor active states).

These NSI states are also denoted as VxVy where Vx refers to the voltage space vector of the upper 'sub-inverter' whereas Vy refers to the voltage space vector of the lower 'sub-inverter', voltage space vector Vi and corresponding switch positions of each 'sub-inverter' are shown in Table 3.

Table 4-3:Switching Vectors of NSI

VxVy	Leg A	Leg B	Leg C	Type
V_7V_0	1	1	1	Zero vectors
V_7V_7	0	0	0	
V_0V_0	-1	-1	-1	
V_1V_0	1	0	0	Upper active vectors
V_2V_0	1	1	0	
V_3V_0	0	1	0	
V_4V_0	0	1	1	
V_5V_0	0	0	1	
V_6V_0	1	0	1	
V_7V_1	-1	1	1	Lower active vectors
V_7V_2	-1	-1	1	
V_7V_3	1	-1	1	
V_7V_4	1	-1	-1	
V_7V_5	1	1	-1	
V_7V_6	-1	1	-1	
V_1V_1	-1	0	0	Same active vectors
V_2V_2	-1	-1	0	
V_3V_3	0	-1	0	
V_4V_4	0	-1	-1	
V_5V_5	0	0	-1	
V_6V_6	-1	0	-1	
V_2V_1	-1	1	0	Middle active vectors
V_2V_3	1	-1	0	
V_4V_3	0	-1	1	
V_4V_5	0	1	-1	
V_6V_5	1	0	-1	
V_6V_1	-1	0	1	

Referring to the 27 switching combinations we can notice that the NSI has two modes of operation. Mode 1, where loads can be supplied simultaneously for only a limited number of vectors (Same Active vectors and Middle active vectors). In mode 2, loads of the NSI can be driven in alternate manner either for all possible combinations or only for the remaining switching combinations from mode 1. It should be noted that in the alternate supply by the NSI (i.e., mode 2), when one load is in active state (i.e., supplied by the NSI) the second load is in zero state (i.e., its three terminals are shorted to one of the DC rails.) and vice versa. The sum of modulation indices of the two 'sub-inverters' can reach up to 1.15.

On the other hand, when loads of the NSI are supplied simultaneously, the middle switches are all ON (i.e., closed) and therefore the NSI behaves as an ordinary two-level inverter supplying two loads in parallel. In this case, modulation indices of each of the two loads can be reach up to 1.15 [26]

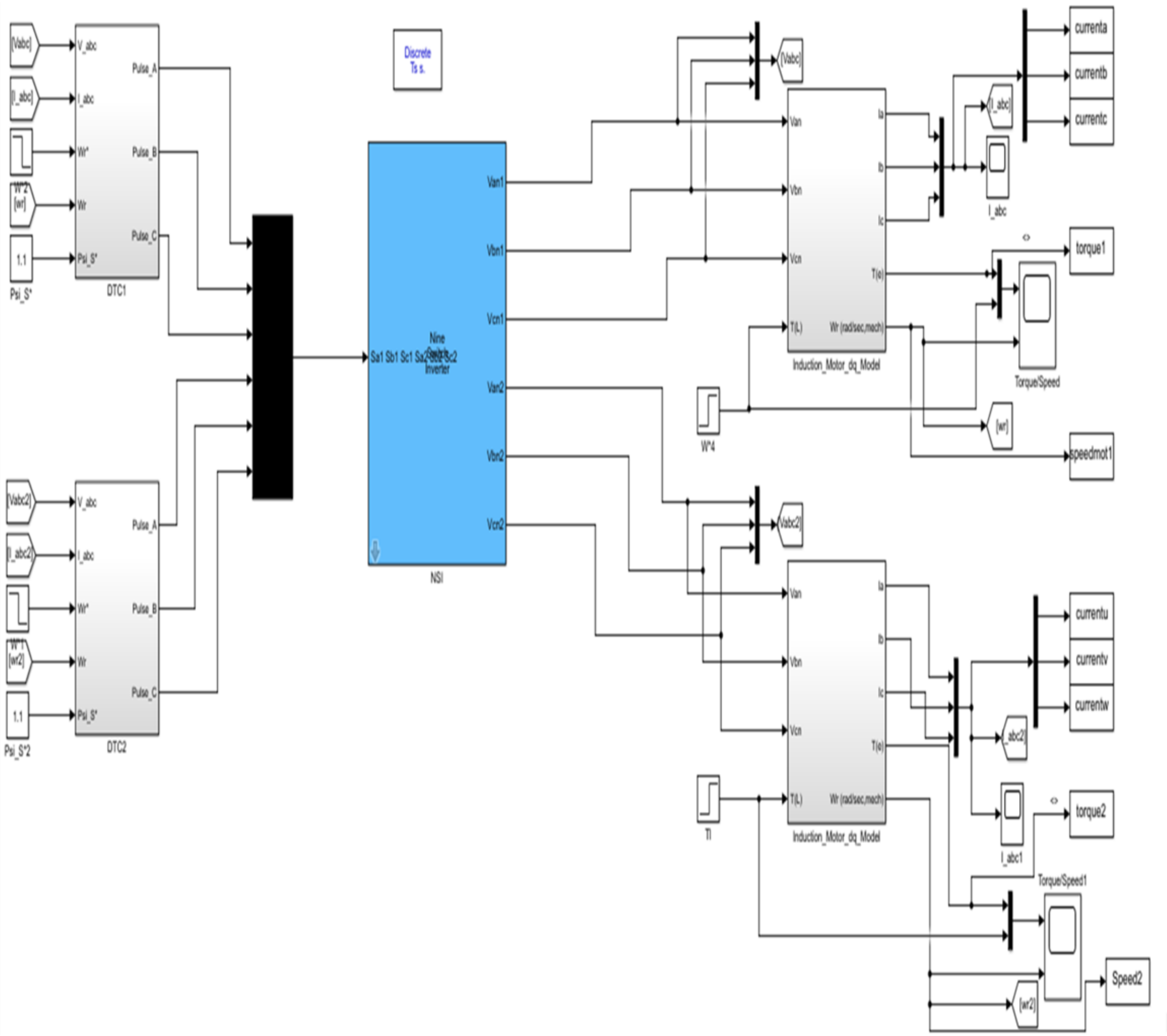

.

Figure 4.3:Simulink model of direct torque control of two induction fed by nine switch inverter

4.9 Simulation and results of direct torque control fed two induction motors by a nine-switch inverter

After running simulation model, we got the following figures

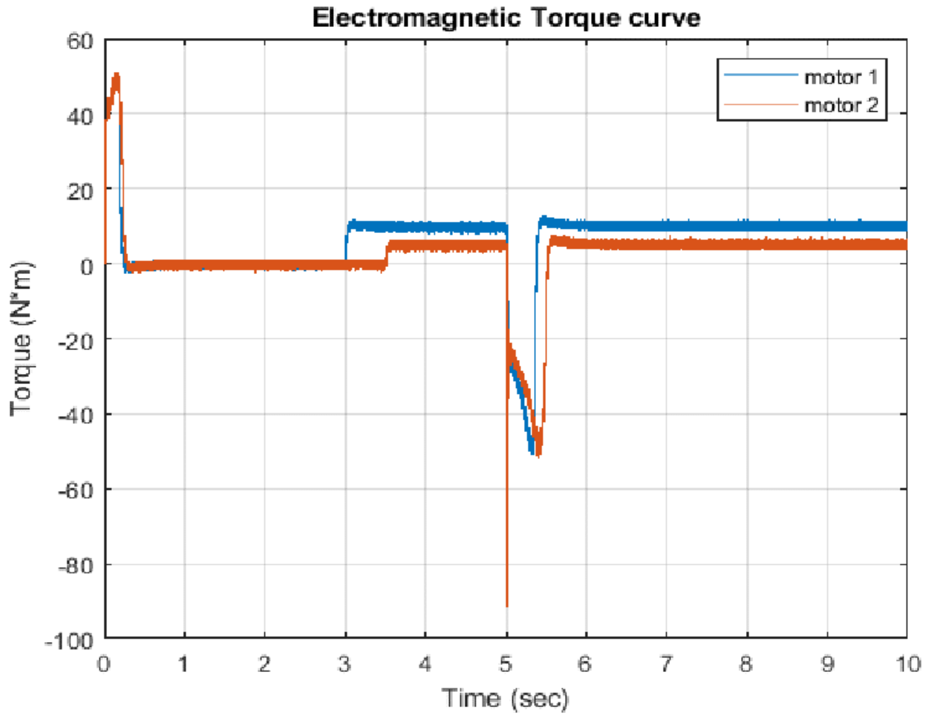

Figure 4.4:Electromagnetic torque of the two induction motor.

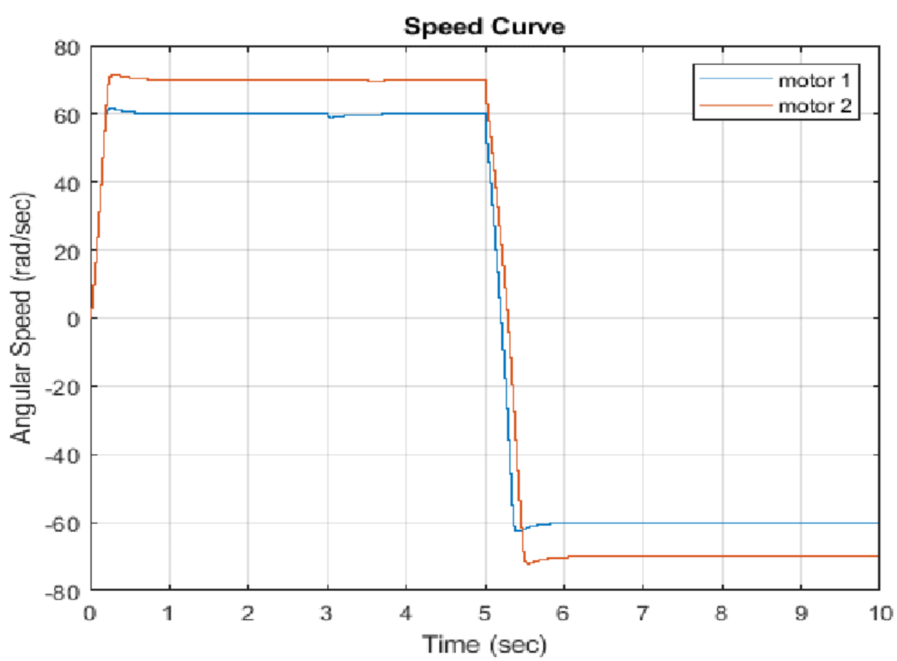

Figure 4.5:Angular velocity of the two induction motor.

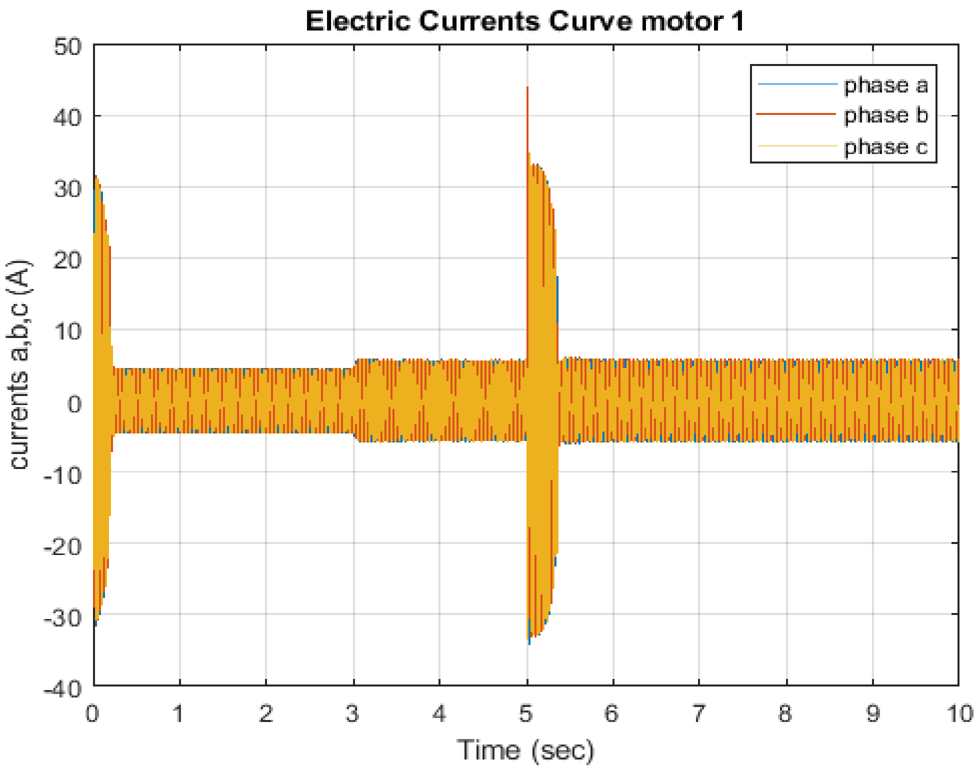

Figure 4.6:Electric current curve motor 1

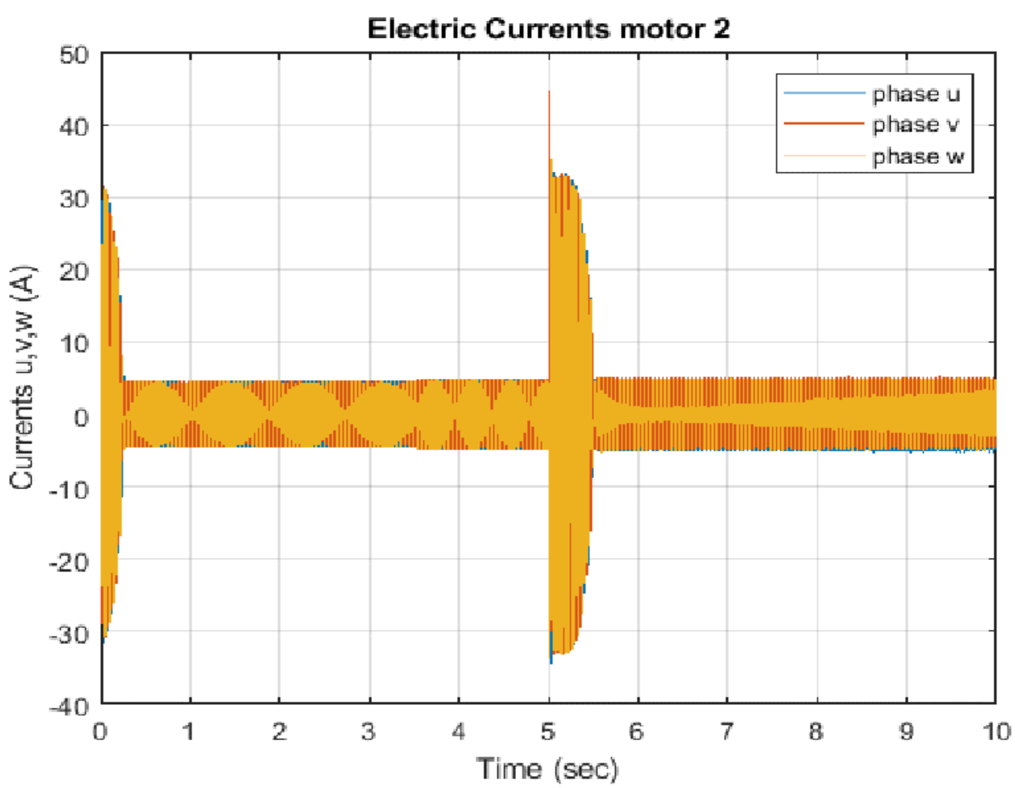

Figure 4.7: Electric current curve motor 2.

4.10 Discussion

Figure 4.4 shows the torque response of the two motors, the torque starts with high values which is an inherent feature in induction motor. After certain time the torque values decreases and settle at zero, the load torques are introduced the torque values increase to reach the load torque and settle at its value, the reversal of speed reference leads to a large decrease in torque reaching negative values due to the abrupt change in speed reference speed.

Figure 4.5 represents the speed response of the two motors, At no load condition, the motors follow their reference speeds, introducing the loads torque cause a decrease in the speed due to the inertia of the loads that act as a damper for the rotor, the speeds increase and return back to their reference values after certain time because of the compensation action of the PI controllers that reduce the speed errors.

Figures 4.6 and 4.7 show the stator current profiles of motor1 and motor2, high starting current can be noticed for both motors which are required to set up the revolving magnetic fields in the air gaps, after certain time the currents settle at small values due to the high impedance value seen by the stator at start up resulting in small currents , after introducing the torque more currents are drawn because the decrease in the impedance value.

4.11 Conclusion

In this chapter, we explained the operation principles of Direct torque control (DTC) method then we presented a modeling of the nine-switch inverter fed two induction motors. To test the performance of the control technique, numerical simulations are performed successfully followed by discussion of obtained results in which separate control of the two motors has been achieved.

General Conclusion

In this thesis, the work presented aims to investigate the control of two independent motors. In order to reduce size and cost of drive system, only nine switches are used (three switches per leg) rather than twelve switches in the classical back to back dual output inverter.

First, a general study of the nine-switch inverter was presented, basic principle of operation and switching signals generation. Two control techniques; Vector and Direct torque control of two induction motors; have been presented and developed. For this, a new pulse-width modulation technique has been used to ensure independent control of the two motors. Simulation study was carried out on the MATLAB / SIMULINK software which proved the validity and effectiveness of the two control methods with the proposed pulse-width modulation technique applied to the nine-switch inverter supplying two induction motors.

Through obtained simulation results presented in previous chapters, we noticed a significant reduction in electromagnetic torque ripples. We can clearly observe excellent current waveform amelioration. In conclusion, it had demonstrated by simulation the performances improvement of the controlling of the two induction motors using a DTC rather than vector control IRFOC technique.

As a further work it can be suggested the following topics:

- Develop a fuzzy logic based- PI controller to improve the speed response;
- Design a control algorithm for DTC that is faster, more accurate while independent control of the two motors is satisfied.
- Implementing the nine-switch inverter in the lab using vector control and DTC schemes;
- Investigating higher level inverter and compare it with nine switch inverter.

References

[1] P. Krause, Analysis of electric machinery, New York: Mc-Graw Hill, 1986.

[2] P. Sen, Principles of electric machines and power electronics, New York: Willey, 1989.

[3] Pitman, Say MG, The performance and design of alternating current machines, London, 2002.

[4] R. Krishnan, Electric Motor Drives - Modeling, Analysis, and Control, 2001.

[5] Kazuo Oka, Kouki Matsuse, "A Nine-Switch Inverter for Driving Two AC Motors Independently," *IEEJ,* vol. I, pp. 94-96, 2007.

[6] Ch.Srinivasulu, E.Parameswara, "SPACE VECTOR MODULATION FOR NINE-SWITCH INVERTER," *International Journal of Modern Trends in Engineering and Research (IJMTER),* vol. 2, no. 6, pp. 595-602, 2015.

[7] Stefania de Oliveira Silva, Washington Luiz Araujo Neves, Wellington Santos Motay, "SPACE VECTOR PWM NINE SWITCH CONVERTER TOPOLOGY," in *XXII Congresso Brasileiro de Automática*, Paraiba,Brazil, 2018.

[8] De Bin Wu, Yongqiang Lang, Navid Zargari, Samir Kouro, Power Conversion and Control of Wind Energy Systems, John Wiley and Sons, 2011.

[9] José Andrés Santisteban, Richard M. Stephan, "Vector Control Methods for Induction Machines," *IEEE TRANSACTIONS ON EDUCATION,* vol. 44, no. 2, MAY 2001.

[10] B Chetate, A Kheldoun, "A method of minimizing the power losses in an induction motor with a squirrel-cage with vector control," *Electrical Technology Russia,* no. 4, pp. 154-165, 2004.

[11] K. Naresh, Vaddi Ramesh,Punya Sekhar, P Anjappa, "SIMULATIONS FOR THREE PHASE TO TWO PHASE TRANSFORMATION," *International journal of emerging Trends in Electrical and Electronics Engineering (IJETEE),* vol. 10, no. 1, 2014.

[12] E. Radwan, N. Mariun, I. Aris S.M , Bashand A.H. Yatim, "IRFOC induction motor with rotor time constant estimation modeling and simulation," vol. 24, no. 4, pp. 1093-1119, 2005.

[13] Salim Djeriou, Aissa Kheldoun, Adel Mellit, "Efficiency improvement in induction motordriven solar water pumping system using golden section search algorithm," *Arabian Journal for Science and Engineering,* no. 43, p. 3199–3211, 2018.

[14] Takahashi, Noguchi T, "A new quick-response and high-efficiency control," *IEEE Transactions on Industry Applications,* vol. 22, no. 5, p. 820–827, 1986.

[15] M.Depenbrock, "Direct self control (DSC) of inverter fed induction machine," *IEEE Transaction on Power Electronics,* vol. 3, no. 4, pp. 420-429, 1988.

[16] Brandstetter P, Chlebis P, Palacky P, "Torque Control of Induction Motor with Direct Calculation of Voltage Vector," *Advances in Electrical and Computer Engineering,* vol. 10, no. 4, pp. 17-22, 2010.

[17] Carmelia S, Maurib M, "Direct torque control as variable structure control," *Electric Power Systems Research,* no. 81, pp. 1188-1196, 2011.

[18] Kuo-Kai S, Juu-Kuh L, Van-Truong P, Ming-Ji Y, Te-Wei W., "Minimum torque ripple design for direct torque control of induction motor drives," *.IEEE Transactions on Industrial Electronics,* vol. 9, no. 57, pp. 3148-3156, 2010.

[19] J. Nash, "Direct torque control, induction motor vector control without an encoder.," *IEEE Transactions on Industry Applications.,* vol. 2, no. 33, pp. 333-341, 1997.

[20] Tiitinen P, Pohkalainen P ,Lalu J , "The next generation motor control method:Direct torque control(DTC)," *European Power Electronics and Drives,* vol. 1, no. 5, pp. 14-18, 1995.

[21] Kazmierkowski MP, Kasprowicz A, "Improved direct torque and flux vector control of PWM inverter-fed induction motor drives.," *IEEE Transactions on Industrial Electronics,* vol. 4, no. 45, 1995.

[22] Buja GS, Kazmierkowski MP, "Direct torque control of PWM inverter-fed AC motors," *IEEE Transactions on Industrial Electronics,* vol. 51, no. 4, pp. 744-757, 2004.

[23] Yuttana K, Suttichai P, Hamid AT, "Modified direct torque control method for induction motor drives .," *Journal of Electric Power Systems,* vol. 10, no. 78, pp. 1712-1718, 2008.

[24] Cherifi Djamila and Miloud Yahia, Direct Torque Control Strategies of Induction Machine: Comparative Studies, January 24th 2020.

[25] Yang M, Tang S, Xu D, "Comments on Antiwindup strategy for PI-type," vol. 2, no. 62, pp. 1329-1332, 2015.

[26] Dehghan S.M ,Mohamadian M and Andersen, "Full space vectors modulation for nine-switch converters including CF & DF modes," in *Proceedings of the IEEE 4th International Conference on Power Engineering and Optimization (PEOCO)*, 2010.